EUROPEAN ORGANIZATION FOR NUCLEAR RESEARCH

THE NOVEL 4 kV, 40 kA CAPACITOR DISCHARGE POWER CONVERTERS
FOR THE PULSED SEPTUM MAGNETS IN THE PS STRAIGHT SECTIONS 16 AND 58

C. Ducastel, J.P. Royer and F. Voelker

ABSTRACT

The requirements imposed on the power converters by operating the PS with periodic sequences of different accelerator cycles are reviewed.

We describe the particular technical solutions which have been developed for performing, simultaneously, high current precision and reproducibility, irregular pulse repetition periods, pulse-to-pulse current reference modulation, and double pulsing within the same accelerator cycle.

New design aspects and operational test results are reported in order to illustrate the progress made by pulsed power converter technology, as well as its interesting potential for applications in the accelerator environment.

CONTENTS

List of figures

List of Tables

1. INTRODUCTION

The Proton Synchrotron (PS) complex at CERN [1], shown in Fig. 1, consists of the following ten accelerators:

- the electron-positron (e^-e^+) 200 MeV and 600 MeV LEP Injector Linacs (LIL);
- the e^-e^+ 600 MeV Electron-Positron Accumulator (EPA);
- the two 50 MeV linear accelerators LI1 and LI2 handling protons and ions;
- the 800/1000 MeV Proton Synchrotron Booster (PSB);
- the 28 GeV/c Proton Synchrotron (PS) itself;
- the 3.5 GeV/c Antiproton Accumulator and Collector (AAC);
- the 200/2000 MeV/c Low-Energy Antiproton Ring (LEAR).
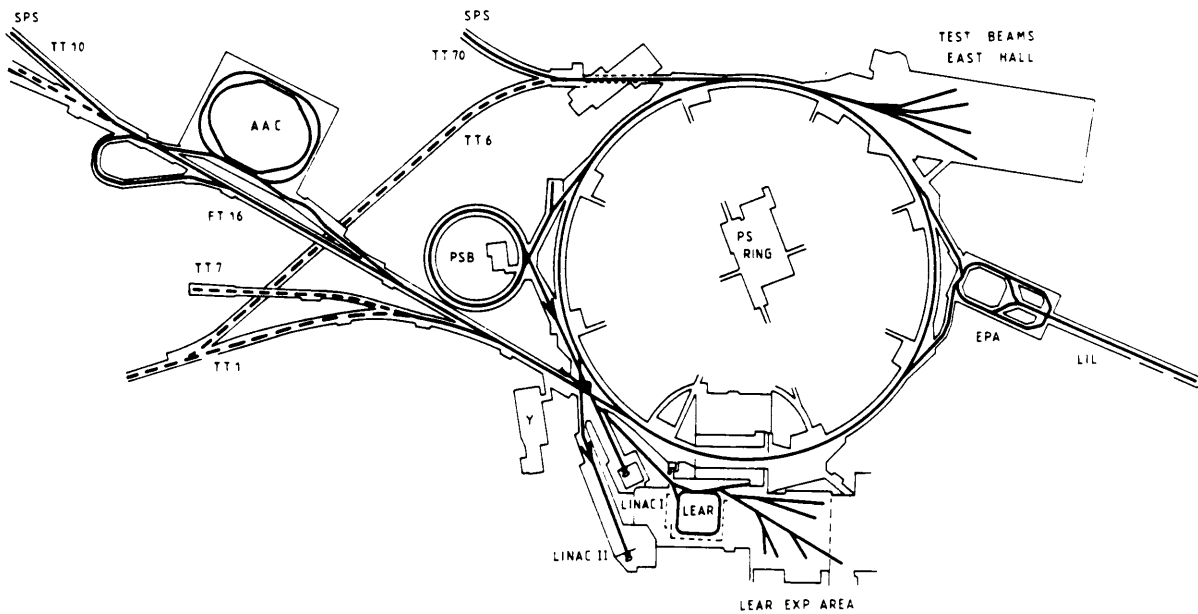
Fig. 1 Layout of the PS accelerator complex at CERN.

Particle beams of different kinds and characteristics are exchanged between the PS and the other accelerators or external beam transport lines, as shown schematically in Fig. 2, for example:

- 800/1000 MeV protons (p) from the PSB to the PS in straight section (SS) 42;
- 24 GeV/c p from the PS SS62 to the East Experimental Area;
- 26 GeV/c p from the PS SS16 to the AAC, where they produce 3.5 GeV/c $\bar{p}$ on a high-density target;
- after collection, accumulation, and stochastic cooling, the 3.5 GeV $\bar{p}$ are reinjected into the PS SS16; there they are either accelerated to 26 GeV/c and transferred from the PS SS58 to the Super Proton Synchrotron (SPS) or decelerated to 600 MeV and ejected from the PS SS26 to LEAR;
- 3.5 GeV/c p from the PS SS16 to the AAC for test purposes;
- 14 GeV/c p and 20 GeV/c ions from the PS SS16 to the SPS, which acts as a 450 GeV/c accelerator for fixed-target physics as well as a 270/350 GeV/c $p\bar{p}$ storage ring and collider;
- 26 GeV/c p from the PS SS16 to the SPS and back to the PS SS58 on subsequent cycles for beam tests to prepare $\bar{p}$ transfers;
- 600 MeV e^+e^- are injected into the PS SS92 and SS74, accelerated to 3.5 GeV/c, and transferred to the SPS from the PS SS58 and SS16. The SPS accelerates these particles to 20 GeV/c for

1

injection into the 50/100 GeV/c Large Electron-Positron storage ring (LEP), which is expected to enter into operation in 1989.

Inside the PS complex the pulsed septum magnets in SS16 and SS58 act as switchyards for different types of particles in both directions, according to an intricate and very flexible scheme of operations.
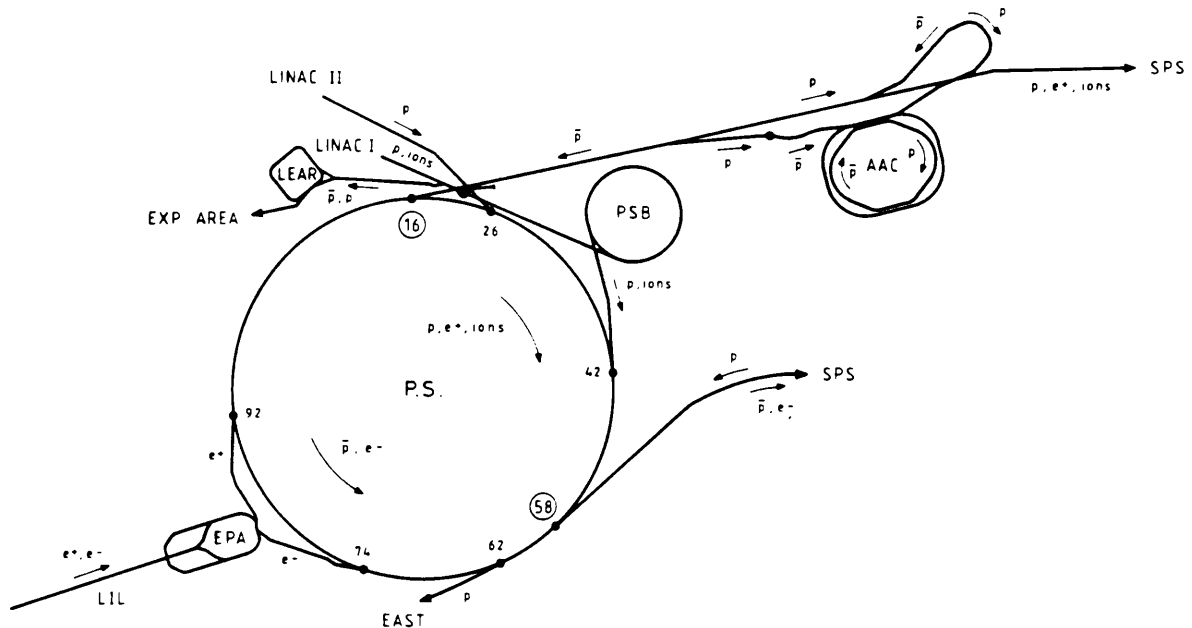
Fig. 2 Functional representation of particle beams handled by the PS accelerator complex.

2. OPERATIONAL REQUIREMENTS

The operation of the Proton Synchrotron [2, 3], is based on repetitive sequences of up to 14 cycles of 1.2/2.4 s duration — for a total length of up to 28.8 s — called supercycles.

The type of cycles which compose a PS supercycle are shown in Table 1.
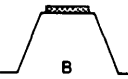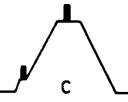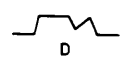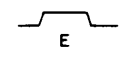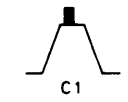
Within a supercycle, during the cycles of types A, C, C1, and E, the septum magnet in SS16 deflects the ejected positive particles (e^+, p, ions) at 3.5, 14, 20, 26 GeV/c, as well as the reinjected negative ones ($\bar{p}$) at 3.5 GeV/c, while the magnet in SS58 handles the ejected negative particles (e^-, $\bar{p}$) at 3.5 and 26 GeV/c and the injected positive ones (p) at 26 GeV/c.

Eight different supercycles have been in operation so far. Some of them are shown in Fig. 3. The pulsed power converters which deliver the excitation current are requested to perform, within a supercycle:

  i) high-current precision and pulse-to-pulse reproducibility;

  ii) one to eight pulse-to-pulse current amplitude modulation;

  iii) irregular pulse repetition periods;

  iv) stable current flat top and double pulses at 30 ms interval during operation with leptons at 3.5 GeV/c.

2

Table 1

Basic PS cycles and septum magnet excitation

Type	Momentum of flat tops (GeV/c)	Length of flat tops (ms)	Particles	Injection energy (GeV)	Cycle duration (s)	Origin → destination	Shape of cycle	Current of septum SS16 (kA)	Current of septum SS58 (kA)
A	14	80	p	0.815/1	1.2	PS → SPS		13.8	-
B	24	600	p	0.815/1	2.4	PS → East		-	-
C	3.5 26.3	120 170	p, p̄	0.815/1/3.5	2.4	AAC → PS PS → SPS PS → AAC		3.5 27 27	34
D	3.5/0.6	100	p̄	3.5	1.2	PS → LEAR		-	-
E	3.5	530	e⁻e⁺	0.5/0.6	1.2	PS → SPS/LEP		3.5	4.4
C1	20	20	ions	-	1.2	PS → SPS		20.8	-
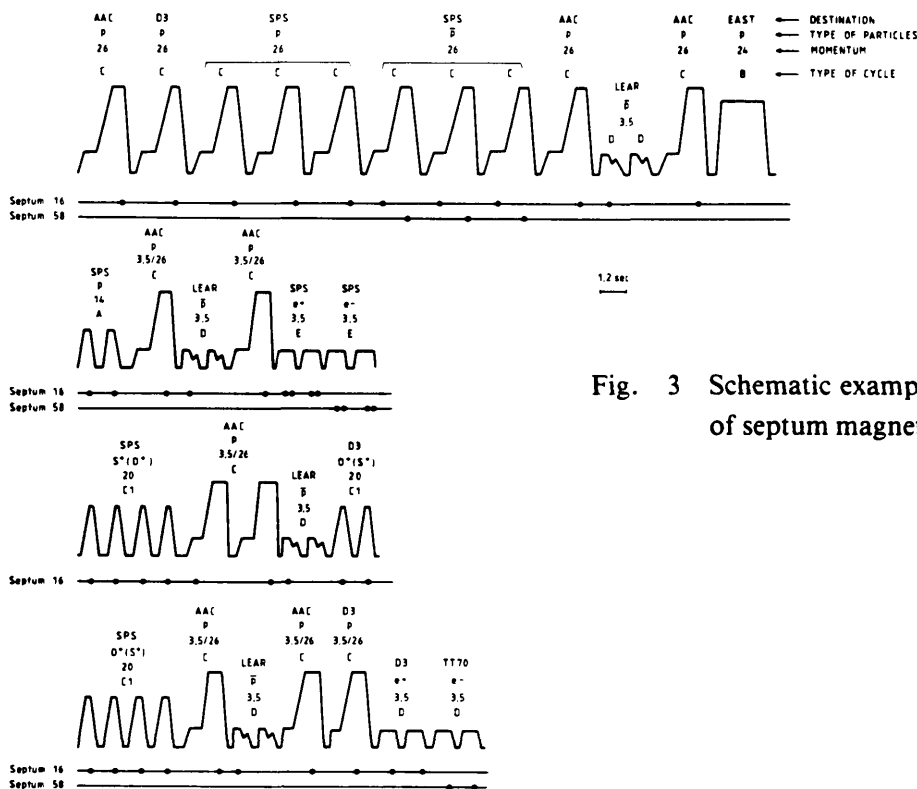
Fig. 3 Schematic example of PS supercycles and of septum magnet operation

3

3. SEPTUM MAGNET CHARACTERISTICS

The septum magnets are mounted in their vacuum tank on a special support equipped with a moving mechanism.

The electrical connection between the magnet and the matching transformer is done with a high-current vacuum feedthrough and a sandwich line. The septum magnets are shown in Fig. 4. The main parameters of the magnets are collected in Table 2.
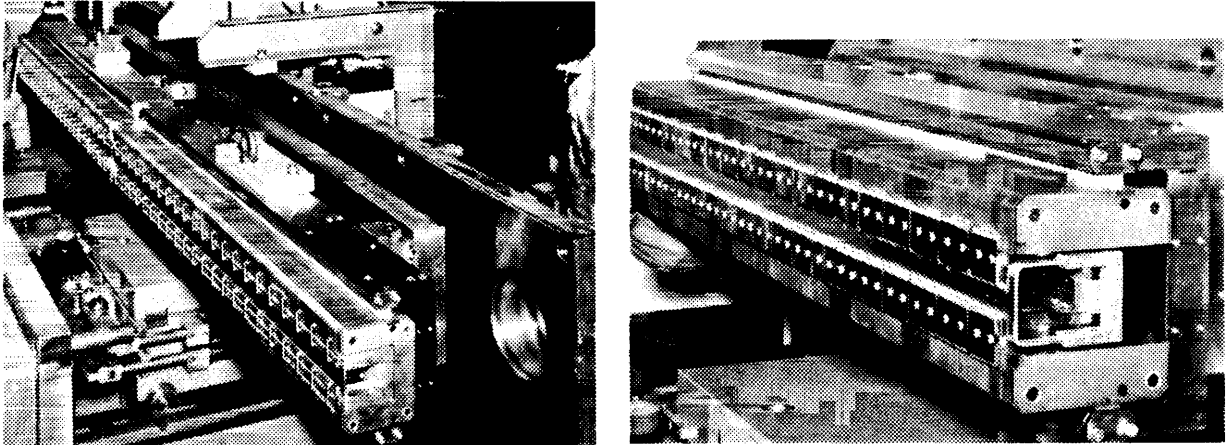
Fig. 4 Electromechanical layout of the septum magnets in PS SS16 and SS58.

Table 2

Septum magnet parameters

		System SS16	System SS58
Physical length	(mm)	2 × 1120	1007
Aperture Horizontal × Vertical	(mm × mm)	61 × 30	70 × 25
Septum blade thickness	(mm)	3	3
Septum copper cross-section	(mm^2)	75	75
Maximum pulse current	(kA)	28	38
Maximum current density	(A/mm^2)	390	520
Maximum magnetic induction	(T)	1.25	1.75
Magnet inductance/resistance	(μH/mΩ)	4.8/1.7	3.4/1.1
Number of turns		1	1
Number of water-cooling ducts		6	6
Mass of septum blade	(kg)	< 2	< 1
Max. magnetic force B.i.l.	(t)	≈ 3.8	≈ 7.3

4. POWER CONVERTER PERFORMANCE SPECIFICATION AND LAYOUT

The basic performance requirements of the power converter are listed in Table 3. The power converter is shown in Fig. 5. Its constructional layout will be described in more detail in Section 11. The pulse-matching and current-measuring transformers as well as the high-current sandwich line are located near to the magnet support.

Table 3

Pulsed power converter specifications

Charging voltage	(V)	≤ 4000
Mean charging current	(A)	≤ 10
Charging time	(s)	≥ 1
Nominal discharge repetition period	(s)	1.2
Capacitance/stored energy in capacitors ($C_1 + C_2$)	(mF/kJ)	1.2/9.6
Peak current on primary/secondary of 12:1		
matching transformer: for the SS16 system	(A)	2500/30000
for the SS58 system	(A)	3330/40000
Current pulse waveform		damped half-sinusoidal
Current pulse half-period	(ms)	≤ 4
Current pulse flat top	(μs)	≤ 300
Current reproducibility and precision $\Delta I/I$	(%)	0.01
Operation at irregular pulse repetition period		Yes
Pulse-to-pulse current amplitude modulation		Yes
Operation with double pulsing and 300 μs flat top		
at 3.5 kA for the SS16 system and 4.4 kA for the SS58 system		Yes
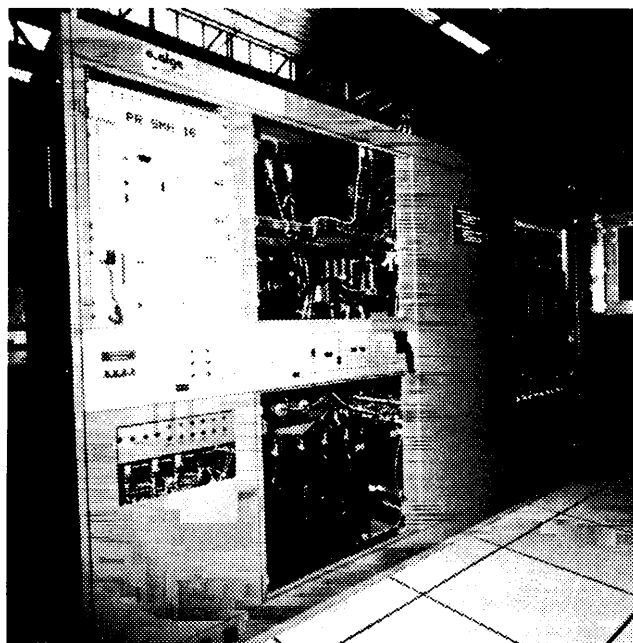
Fig. 5 Layout of pulsed power converter.

5

5. CIRCUIT LAYOUT AND MODE OF OPERATION

The power section is shown schematically in Fig. 6.
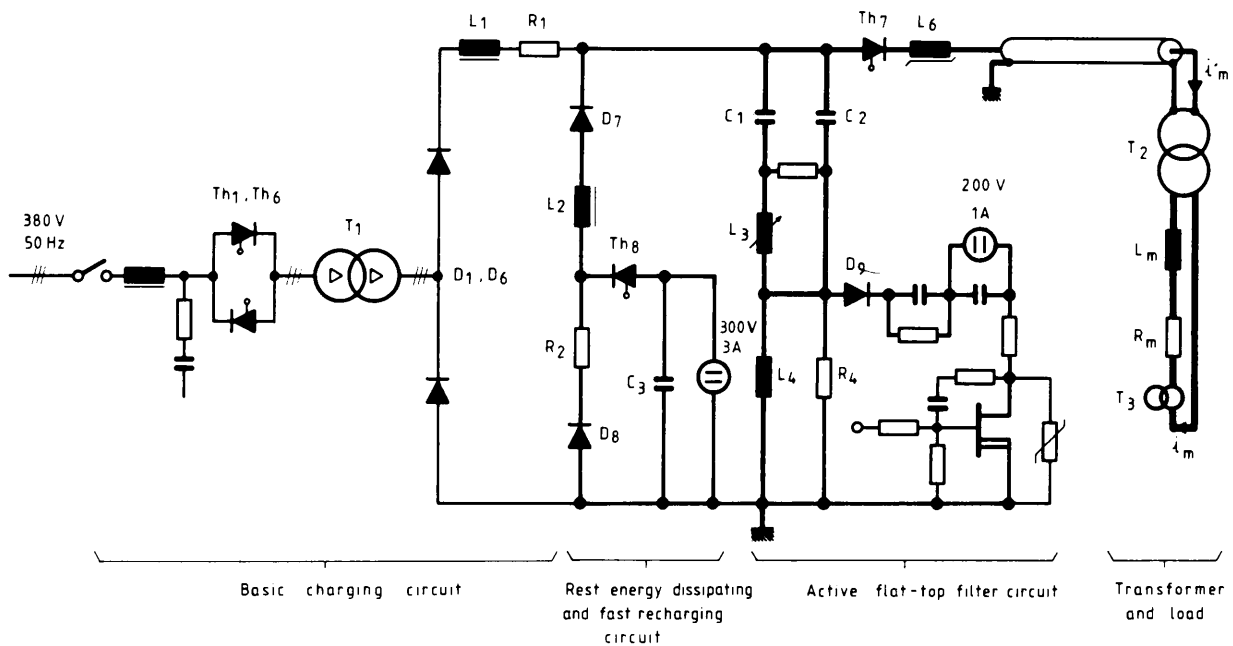
Fig. 6 Schematic circuit diagram of pulsed converter power section.

The capacitors C_1, C_2 are charged and then discharged into the load according to an external synchronizing pulse sequence.

An a.c. thyristor controller Th_1, Th_6 on the primary of a stepping up 3-phase transformer T_1, through the HV rectifier D_1, D_6 provides for linear charging of the energy storage capacitors C_1, C_2 up to the preselected voltage and for final voltage stabilization.

The HV thyristor Th_7 discharges the capacitors into the primary of a 12:1 pulse-matching transformer (T_2) via low-inductance cables.

The capacitors C_1, C_2, the chokes L_3, L_4, as well as the equivalent load impedance, are part of a pulse-forming network, which delivers a half-sinusoidal current waveform and a superimposed adjustable third harmonic.

Fine pulse flat-top regulation is achieved by means of an active filter with a MOS transistor amplifier, connected in parallel with the insertion impedance R_4, L_4.

Owing to the pulse-to-pulse current modulation requirement, the rest capacitor energy after the current pulse has to be dissipated in the circuit R_1, L_1 and R_2, L_2.

When a second current pulse has to be delivered, 30 ms after the first one, then thyristor Th_8 resonantly recharges the capacitors via the circuit C_3, L_2. A low power voltage source recharges the buffer capacitor C_3 after the second current pulse.

The basic voltage and current waveforms of the pulsed power converter are shown in Fig. 7.

u_C: 800 V/div; i_C: 5 A/d; 0,1 s/d i_m: 5 kA/d; 0,5 s/d
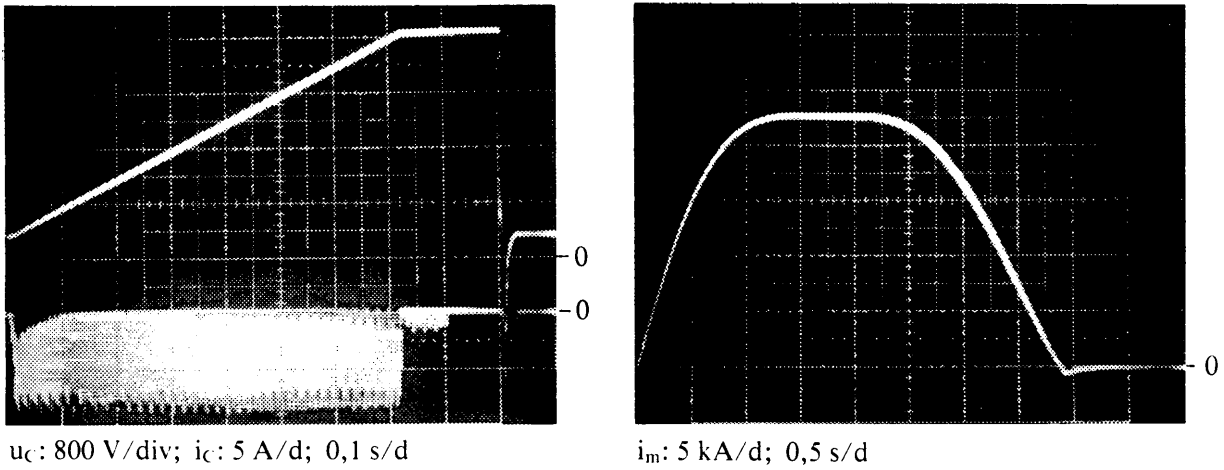
Fig.   7   Basic waveforms of pulsed power converter:
a) capacitor charging current and voltage;
b) septum magnet current pulse.

6.   BASIC POWER SECTION

For the sake of simplicity, and unless specified otherwise, reference will be made from now on to the power converter of the septum magnet in SS16; the design and layout of the SS58 system is basically the same. The design aspects are discussed with reference to Fig. 6. The main elements of the basic power circuit are shown in Table 4.

Table 4

Components of basic power circuit

Components		Characteristics
Three-phase transformer T_1:		
connection		D-D
power	(kVA)	63
primary/secondary voltage	(V)	380/3100
primary/secondary current	(A)	46/12
type		dry-class F
a.c. thyristor controller Th_1-Th_6		SKKT 131/14 on P3 heat sink
HV avalanche diode rectifier D_1-D_6		SKNa 20/17 on K3 heat sink
Smoothing choke L_1	(mH)	100
Resistor R_1	(Ω)	4
Energy-dissipating path choke L_2	(mH)	5
Resistor R_2	(Ω)	4
HV diode D-		R 720.44
Energy storage capacitors C_1	(μF)	685
C_2	(μF)	515
Third harmonic choke L_3	(μH)	560
Active filter choke L_4	(μH)	50
Resistor R_4	(Ω)	3
Discharge HV thyristor Th-		W-T9 Go 44-6
di/dt limiting reactor L_6	(μH)	100/5

7

6.1 Capacitor charge and discharge circuits

The design of the pulse-shaping discharge network is treated in Appendix A. The capacitor-charging circuit consists of the input a.c. filter, the thyristor controller, the 3-phase transformer and avalanche diode rectifier, and the smoothing and damping circuit R_1, L_1.

The charging current is driven by the voltage difference between the rectified portions of the secondary transformer line-to-line voltage as a function of the firing angle and the actual capacitor voltage. This current consists of a 300 Hz pulse train, where the peak and form factors vary in the course of the charging process. The uniformity of consecutive current pulses depends on the symmetry and tracking of the gate control set as well as on the symmetry of the a.c. power circuit. For a charge voltage U_C of the energy storage capacitor, the peak discharge current $\hat{i}_m'$ and its duration $T/2$ are given by the approximate relations:

$$\hat{i}_m' \approx k_1\, U_C\, \sqrt{C/L}\; e^{-RT/8L}$$

$$T/2 \approx k_2\, \pi\, \sqrt{LC}\,,$$

where $C = C_1 + C_2$.

The coefficients $k_1 = 1.3$ and $k_2 = 1.15$ have to be applied owing to the pulse-forming network with 3rd harmonic.

The parameters R and L are the total circuit resistance and inductance seen from the primary of the matching stepping-down transformer, with the ratio of N_1/N_2 turns. This ratio is selected on the basis of the load impedance, the peak magnet current, and the maximum pulse duration. In fact, to reduce thermal and mechanical stresses on the septum magnet, the current pulse should be as short as possible; on the other hand, the current flat top produced by the active filter has a duration of the order of $T/50$ at maximum current. Following these considerations $N_1/N_2 = 12$ and $T/2 \leq 4$ ms have been selected for this power converter, where $\hat{I}_2 \leq 29$ kA (39 kA for the SS58 magnet).

For reasons of standardization, identical matching transformers are used on the systems in SS16 and SS58.

A maximum charging voltage of $U_C \leq 4$ kV allows the use of a single discharge thyristor — therefore avoiding lossy and leaking voltage-sharing resistors for series connection — provided the time when full voltage is applied is limited by a suitable timing sequence.

Reliable and cost-effective 4 kV capacitors for this type of operation are available from different manufacturers.

6.2 Pulse transmission and sandwich lines

The power converter is connected to the pulse-matching transformer via parallel connected HV cables, which are designed for low impedance as compared with that of the load as seen from the primary.

The characteristics of the pulse transmission cables are given in Table 5.

Table 5

Characteristics of pulse-transmission cables

Manufac-ture	Type	Number of cables in parallel	Diameter of int./ext. conductor (mm)	Cross-section of int./ext. conductor (mm^2)	Number of braids of int./ext. conductor	Operating/ test d.c. voltage (kV)	Resistance/ inductance ($\Omega \cdot km^{-1}$/ $\mu H \cdot km^{-1}$)	Min. bending radius (m)
PASTA-I	Coaxial Cu conductor PVC insulation	(SS16) 2 (SS58) 3	14.5/24	42/60	198/54	5/11	0.8/150 at 20°C (shorted end)	0.45

The cables are of the coaxial type, while other similar pulsed systems make use of simpler 4 core cables with diametrically opposite pairs of conductors in parallel. The secondary of the transformer is connected to the magnet vacuum feedthrough via a high-current sandwich line made of copper plates, shown in Fig. 8. The sandwich line consists of two rigid and two flexible segments in alternation to permit the magnet tank to move and facilitate assembly/disassembly operations.

The sandwich line, whose characteristics are given in Table 6, provides as low as possible total additional impedance on the secondary of the matching transformer.

The electrodynamic forces during the current pulse are absorbed by the clamping and supporting structure, keeping to a minimum the stresses on the delicate vacuum feedthrough and on the shock-sensitive current measuring transformer.
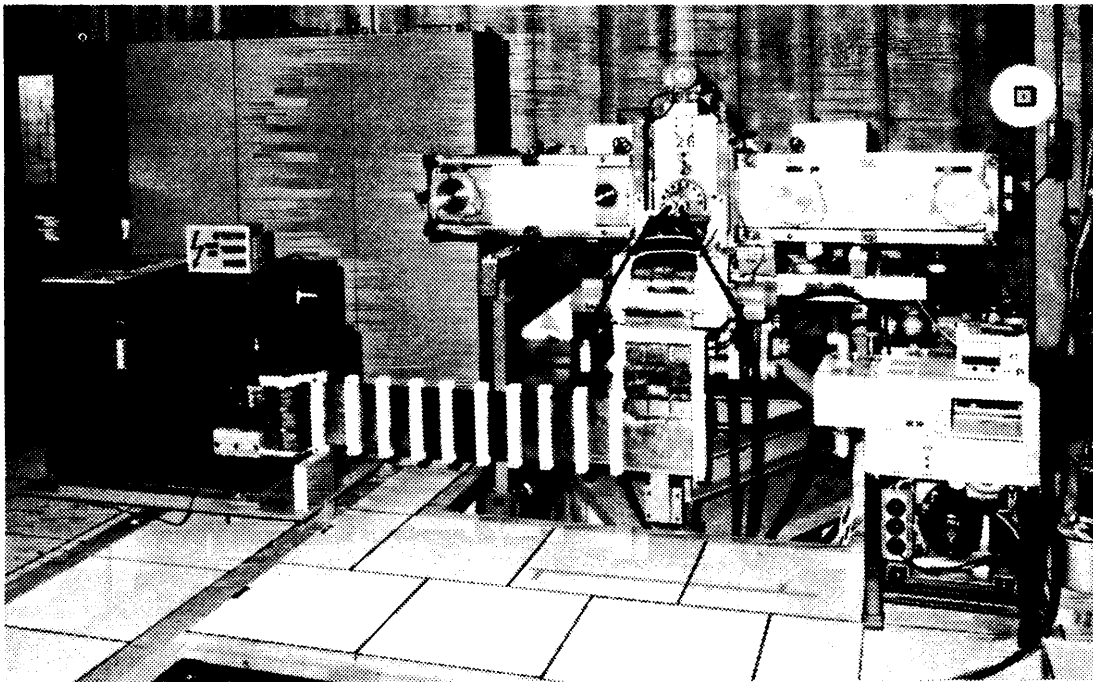
Fig. 8 Electromechanical assembly of the septum magnet in PS SS16 showing (from the left) the pulse-matching and measuring transformers, the high-current sandwich line, the magnet support and vacuum tank.

Table 6

Characteristics of the high current sandwich line

	Total length (m)	d.c. resistance at 20°C ($\mu\Omega$)	Inductance at 1 kHz (μH)	Dynamic force at Î (kN/m)	Conductor cross-section (mm^2)	Max. operating temperature near feedthrough (°C)	Cooling
SS16	2.60	150	0.1	14	1500 (6 × 250)	40	Natural air convection
SS58	1.90	100	0.08	23			

6.3 Pulse-matching transformer

When the amplitude and the repetition period of the unidirectional current pulse are modulated within supercycles, reproducibility in the 0.01 to 0.1% range can be affected by the apparent variation of the transformer turns ratio due to magnetic effects.

Great attention has therefore been devoted to the design of the pulse-matching transformer in collaboration with industry. The three-limb core is composed of a grain-oriented lamination cut at 90°; the central limb carries the cylindrical windings designed for very low stray inductance and losses.

The two secondary windings, connected in parallel, are physically interleaved with the primary HV winding divided into three parts.

The conductor material is copper Litz for the primary and wide copper ribbon for the secondary winding. The insulation is made of Nomex.

Following comparative evaluation tests, an air gap of 2 mm has been inserted in each limb in order to reduce the effects of the varying remanent magnetic induction.

Two slits have been included in the air gap of the external limbs for field measurements by means of Hall plates.

The transformer is shown schematically in Fig. 9 and its characteristics are given in Table 7.
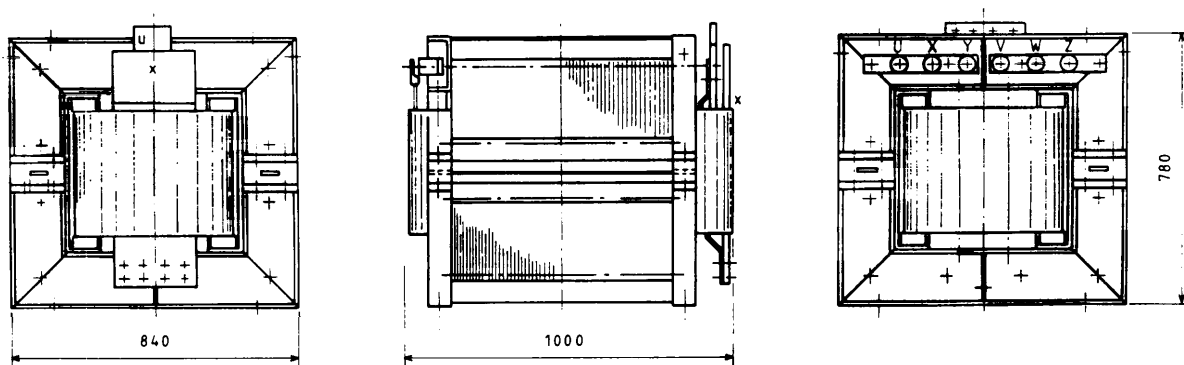
Fig. 9 Construction of pulse-matching transformer.

Table 7

Construction of pulse-matching transformer

Manufacturer		Trasfor/CH
Type of construction/insulation/lamination		dry/class F/M5T30
Effective iron cross-section of external/central limb	(cm^2)	1000/2000
length of magnetic circuit ℓ_i	(mm)	1860
Geometrical air gap ℓ_a	(mm)	4
Number of primary/secondary turns		3 × 24/2 × 2
Turns ratio N_1/N_2		12
peak/effective primary current	(A)	3330/167
Peak/effective secondary current	(A)	40000/2000
Primary/secondary peak voltage	(V)	4000/333
Total cross-section of primary/secondary winding	(mm^2)	3 × 80/2 × 1440
Equivalent resistance R"$_T$ at 115 °C	($\mu\Omega$)	105
Equivalent resistance X"$_T$ at 50 Hz	($\mu\Omega$)	48
Magnetizing inductance L_0	(mH)	32
Dimensions (W × D × H)	(mm^3)	840 × 1000 × 780
Weight	(kg)	3200
Resistance R_0 (idle losses) at U = 1.2 kV, 50 Hz	(Ω)	436

The magnetizing and hysteresis curves, measured by the manufacturer, are shown in Figs. 10 and 11.
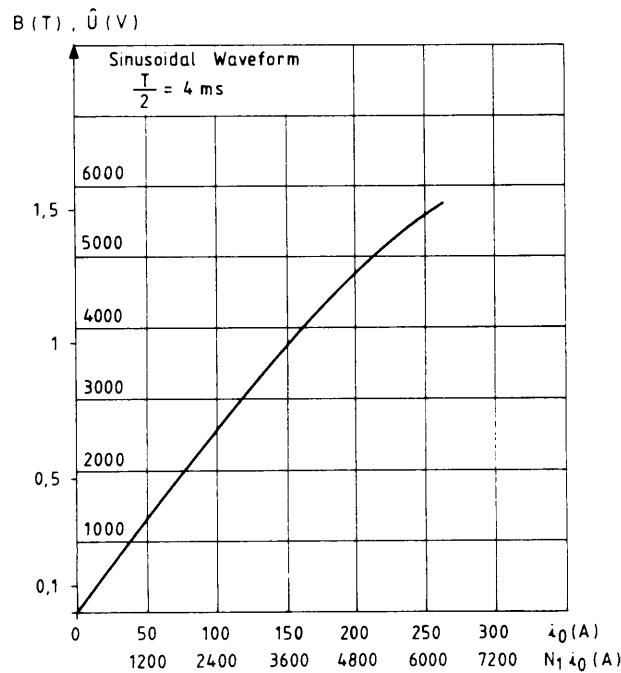
Fig. 10 Measured (50 Hz) magnetizing curve of pulse-matching transformer.

11

u = 1200 V r.m.s.; 5 ms/d $\hat{B}$ = 1,13 T; I_0 = 168 A r.m.s.
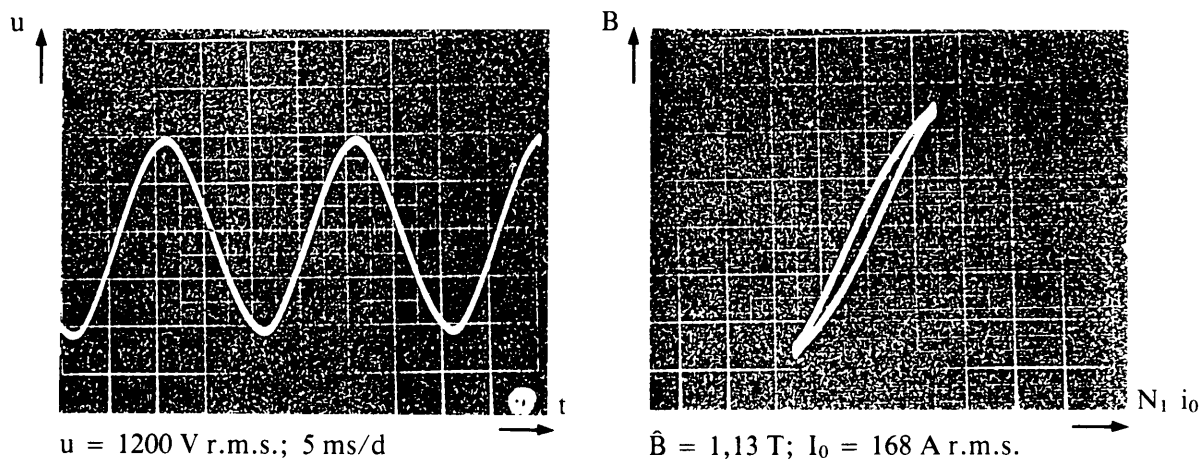
Fig. 11   Measured hysteresis curve of the transformer core at 50 Hz, corresponding to a charging voltage U_C = 4240 V and a magnetic induction $\hat{B}$ = 1.13 T for a current pulse half-period $T/2$ = 4 ms.

6.4 Current-monitoring transformer

The current in the septum magnet is monitored by means of a toroidal transformer installed between the pulse-matching transformer and the high-current sandwich line.

The quality of this device is of utmost importance to obtain the specified current reproducibility and precision. Its characteristics are summarized in Table 8.

Table 8

Characteristics of magnet current monitoring transformer

Manufacturer	Model	Output (V/A)	Max. peak current (kA)	Droop (%/ms)	$(I\cdot\tau)_{max}$ (A·s)	Max. r.m.s. current (A)	Output impedance (Ω)
Pearson/US	2093	0.001	500	0.09	1200	2500	1

7. DOUBLE-PULSE GENERATION

7.1 Fast recharge circuit

The auxiliary circuit required to recharge within 30 ms the energy-storage capacitor (C_1 + C_2) and to produce a second current pulse at ~ 3.5 kA (~ 4.4 kA for the SS58 system) consists of:

i) an industrial power supply, which keeps the electrolytic buffer capacitor $C_3 \gg$ (C_1 + C_2) charged at a preselected voltage.

ii) a LV thyristor Th_8, which initiates the resonant recharge via the inductance L_2.

12

Theoretically the recharge time is

$$T_r \simeq \pi \sqrt{L_2 \frac{(C_1 + C_2)C_3}{(C_1 + C_2 + C_3)}} = 8 \text{ ms} .$$

In practice, transients of the voltage at $(C_1 + C_2)$ at present increase the recharge time to $\sim$ 20 ms. The characteristics of the few extra components required for the double-pulse fast recharge circuit are collected in Table 9.

The operation of the double-pulse generator is illustrated in Fig. 12.

Table 9

Components of double-pulse fast-recharge circuit

Component		Type
Auxiliary power supply		DCR 300/3B
Buffer capacitance C_3	(mF/V)	23.4/350
Recharge thyristor Th_8		DCR 807 SM2323-7845
Blocking diode D_8		DS 912 SM3318-7843

10 ms/d   0,2 s/d
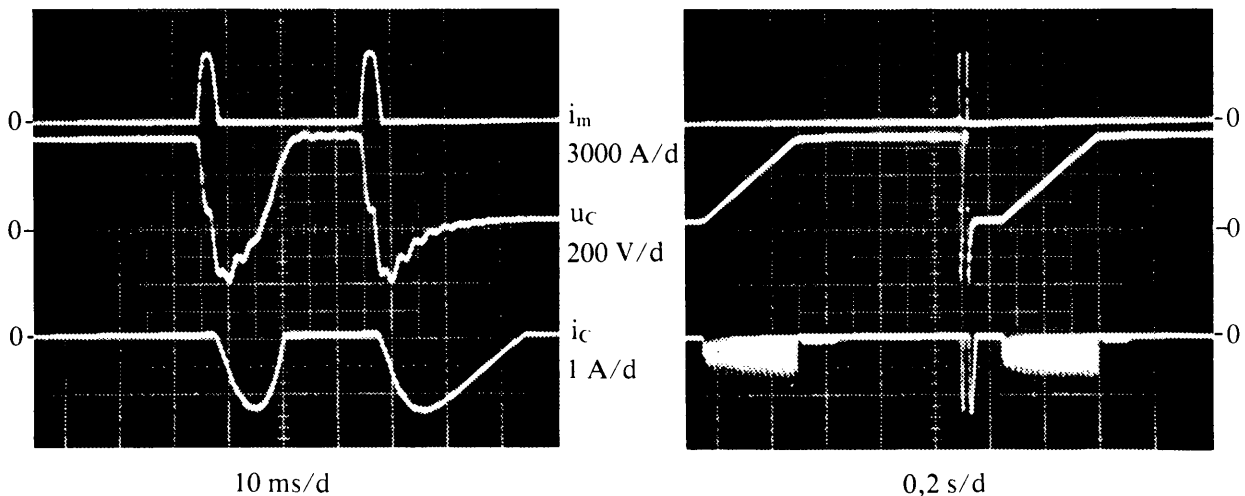
Fig. 12 Waveforms illustrating the operation of the double-pulse generator:

i_m = septum magnet current

u_c = voltage at the energy storage capacitor $(C_1 + C_2)$

i_c = charging current of $(C_1 + C_2)$.

13

7.2 Control of double-pulse mode

The double-pulse mode, with 30 ms time between pulses, can be requested by operation provided that:

i) a lepton cycle at 3.5 GeV/c is foreseen and

ii) the magnet current reference is lower than 4 kA.

In the case of a double-pulse request the appropriate voltage reference and timing are transmitted to the auxiliary circuit for fast resonant recharging of the capacitors.

The double-pulse mode control is shown schematically in Fig. 13.
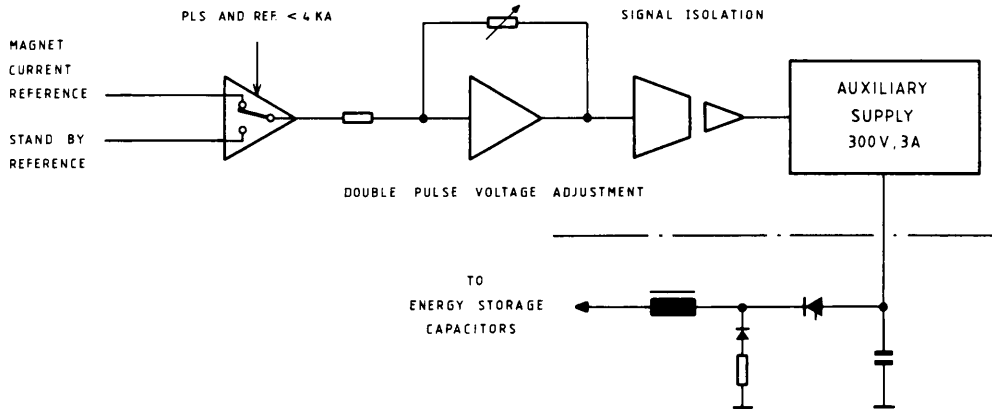
Fig. 13   PLS (Program line sequencer) driven double-pulse mode control principle.

8. ACTIVE CURRENT FLAT-TOP FILTER

8.1 Power circuit and mode of operation

The power circuit of the active filter is shown schematically in Fig. 14, while Fig. 15 shows the characteristics of the load impedance as seen at different points of the circuit.
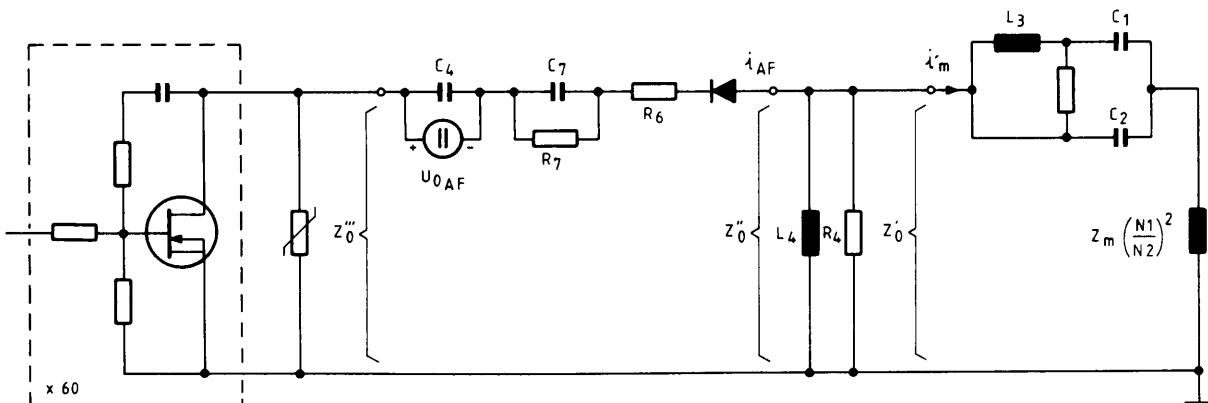
Fig. 14   Diagram of active filter power circuit.
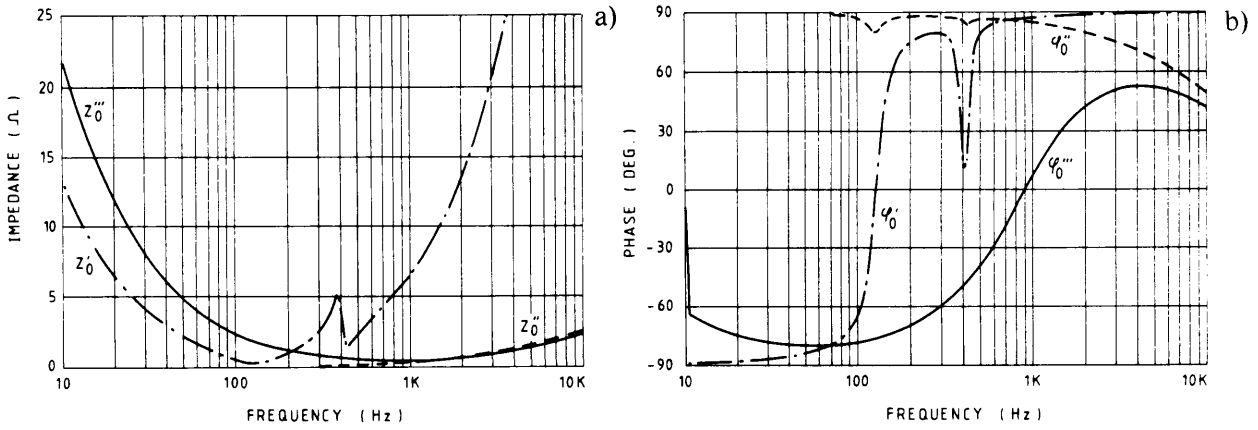
Fig. 15   Load impedance amplitude a) and phase b) as a function of frequency.

The main power components of the active filter circuit are listed in Table 10.

Table 10

Active filter power components

Choke L_4 (μH)	Resistance R_4 (Ω)	Buffer capacitor C_4 (mF)	Coupling impedance R_7, C_7 (Ω/μF)	Current limiting resistor R_6 (Ω)	Auxiliary supply U_{OAF} (V/A)	MOS power transistors
50	3.4	19.5	46/680	0.4	200/1	BUZ 45

It is assumed that the drift correction circuits, which will be described in Section 9, keep the natural capacitor discharge current peak consistently above the required flat-top level. The active filter amplifier will then divert the excess current and precisely regulate the flat-top current.

The maximum nominal current capability of the amplifier power stage is $\sim$ 250 A peak and the impedance ratio $|Z_0'|/|Z_0''|$ between 1 and 5 kHz is $\approx$ 20. Consequently the active filter will typically cover a range of $\leq$ 0.4% of the peak magnet current. When the voltage at the capacitors becomes too high, the active filter amplifier loses control and the magnet current recovers the natural discharge waveform.

The peak voltage across the active filter amplifiers, which is the sum of the auxiliary supply voltage U_{OAF} and of the voltage at the insertion choke, is clamped by voltage-limiting devices (GE-MOV).

The active filter amplifier consists of six modules each carrying ten MOS power transistors in parallel, which present high input impedance and wide bandwidth. The characteristics and operating capability of MOS power transistors used under pulsed conditions are illustrated by the diagrams shown in Fig. 16.

15
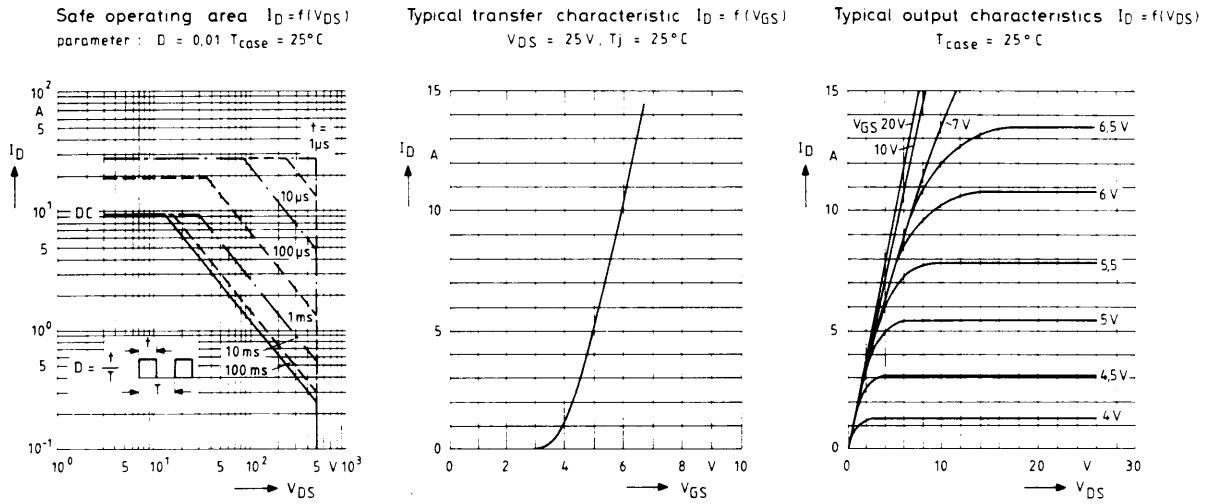
Fig. 16 BUZ45 MOS power transistor characteristics.

Some typical waveforms illustrating the mode of operation of the active filter are shown in Fig. 17.

0,5 ms/d
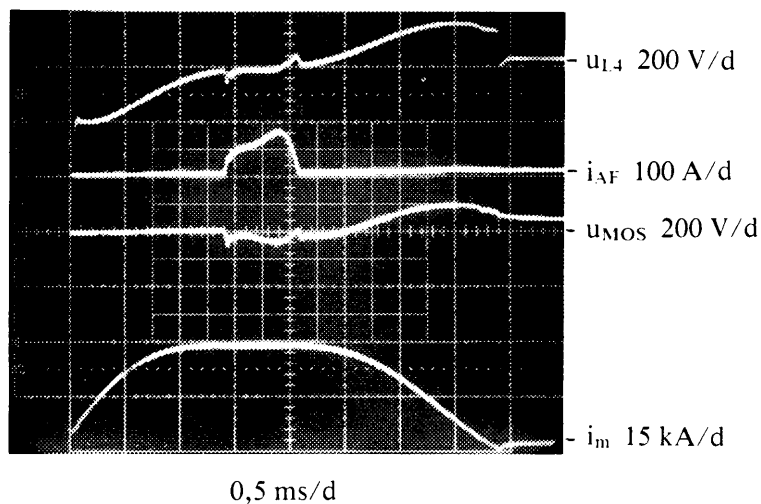
Fig. 17 Waveforms of the active filter power circuit:

u_{L4} : voltage across the insertion choke L_4;

i_{AF} : active filter amplifier current;

u_{MOS} : voltage at the MOS transistor amplifier;

i_m : septum magnet current.

The operation of the active filter during a supercycle with modulation of the magnet current amplitude, and in the case of double pulsing at 3.5 kA and 30 ms interval, is shown in Fig. 18.

0,5 ms/d   5 ms/d
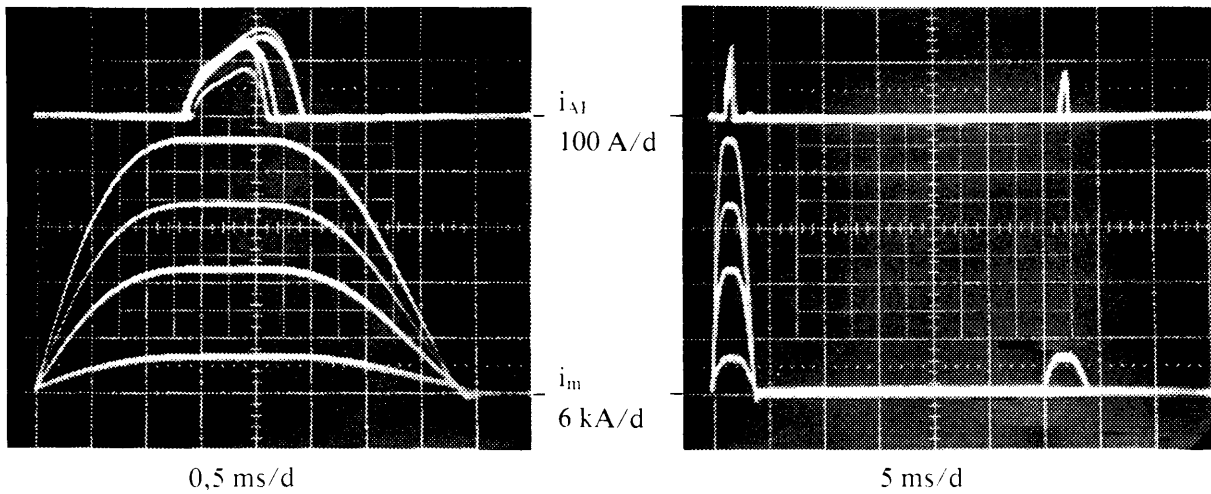
Fig. 18   Operation of the active filter during a supercycle including magnet current pulses at 3.5, 14, 20, 27 kA as well as double pulses at 3.5 kA.

8.2 Active filter regulation

A functional block diagram of the active filter regulation is shown in Fig. 19, while a schematic diagram of the regulation and power stage is shown in Fig. 20.
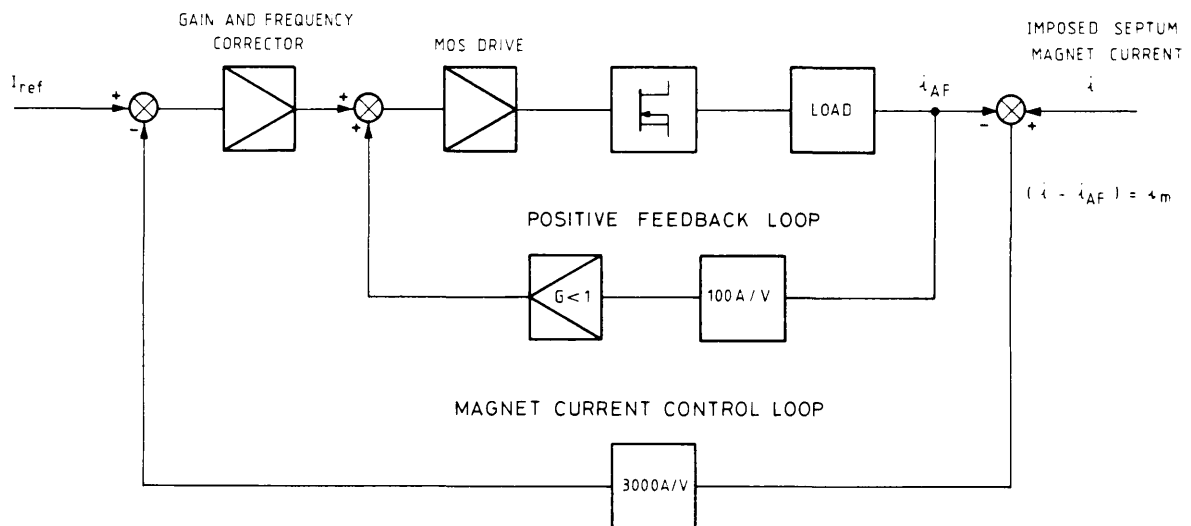
Fig. 19   Principle block diagram of active filter regulation.
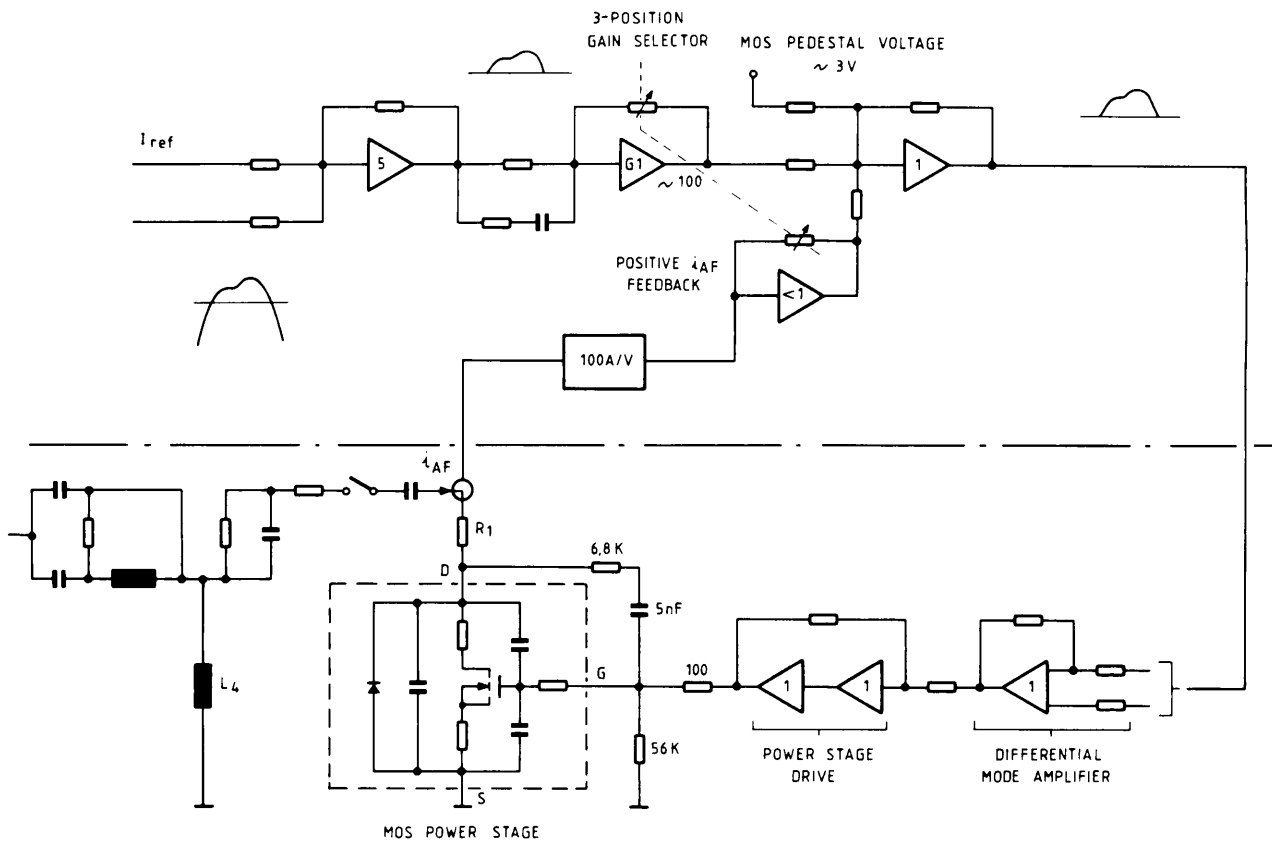
Fig. 20 Schematic diagram of active filter regulation and power stage (waveforms are for $i_{FA} \simeq 0$).

The magnet current reference is compared with the natural capacitor discharge current; and the error signal, after having passed a frequency-response corrector, feeds the amplifier driving the MOS power stage.

The loop gain is automatically adjusted in three steps corresponding to whether the magnet current reference is in the lower, middle, or upper third of its maximum value. A small part of the active filter current signal is positively fed back to obtain higher loop gain and sufficient phase margin.

The drive signal to the MOS power stage passes a differential high input impedance amplifier to avoid earth loop problems.

9. GENERAL CONVERTER REGULATION

The general regulation of the pulsed converter has been functionally divided into two parts which are described in the following paragraphs, namely the regulation of the capacitor voltage and the correction for possible drift effects in order to maintain a suitable active filter operating point despite the varying magnet current and pulse repetition period.

A diagram of the principles of the pulsed power converter regulation, is shown in Fig. 21.

18
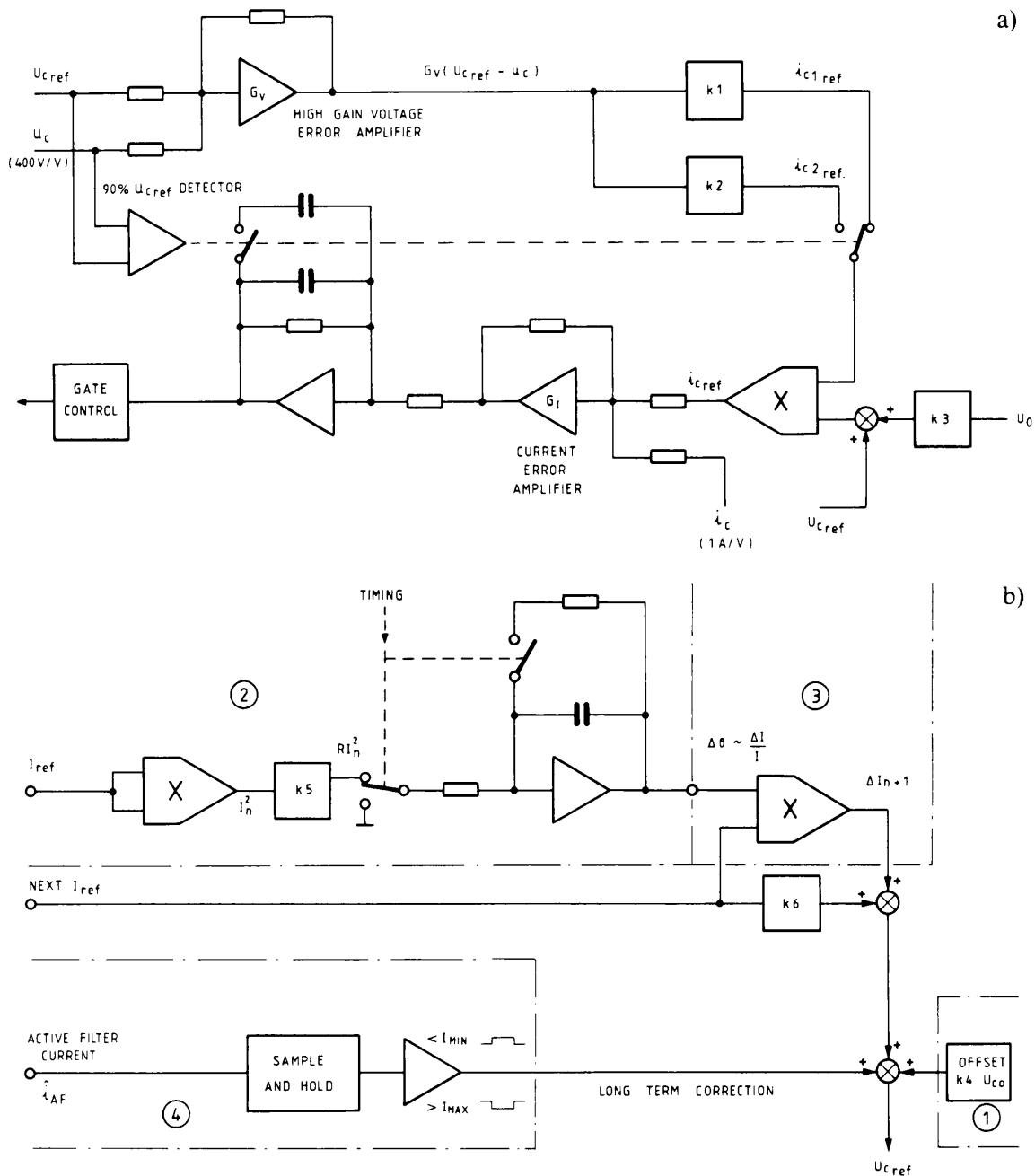
Fig. 21   Principle diagram of the pulsed power converter regulation: a) capacitor charging control, b) auxiliary correction circuits.

9.1 Charging voltage and current control

Charging voltage and current control is obtained by two cascaded regulation loops.

A high gain proportional voltage error amplifier compares the reference capacitor voltage $U_{C_{ref}}$ with the actual voltage u_C. The current reference is derived from its output for each of the three charging stages:

i) the capacitor is charged up to $\sim$ 90% of $U_{C_{ref}}$ at full current $i_{C1_{ref}}$ during about 0.8 s,

ii) the current is then reduced to $i_{C2_{ref}}$ and charging is completed within 0.2 s,

iii) finally, once the voltage error amplifier comes out of saturation, a very small leakage current is delivered to stabilize the voltage at $U_{C_{ref}}$ within a few parts in a thousand.

19

The current reference is commutated from $i_{c_{1_{ref}}}$ to $i_{c_{2_{ref}}}$ by FET switches driven by a comparator. At the same time the frequency corrector of the current control loop is modified to optimize transients. The current control loop feeds the gate control set for the primary thyristor controller.

A roughly constant charging time over the full capacitor voltage range is obtained by deriving the current reference from the voltage error amplifier according to the following relation: $i_{c_{ref}} = (U_{C_{ref}} + k_3 U_0)(i_{c_{1,2_{ref}}})$. The operation of the charging voltage and current regulation are shown in Fig. 22.

u_C with
5,81 V
compensation

at 27 kA
at 20 kA
at 13 kA

u_C

u_C: 20 V/d; i_C: 5 A/d; 0,1 s/d i_C: 5 A/d; u_C: 800 V/d; 0,1 s/d
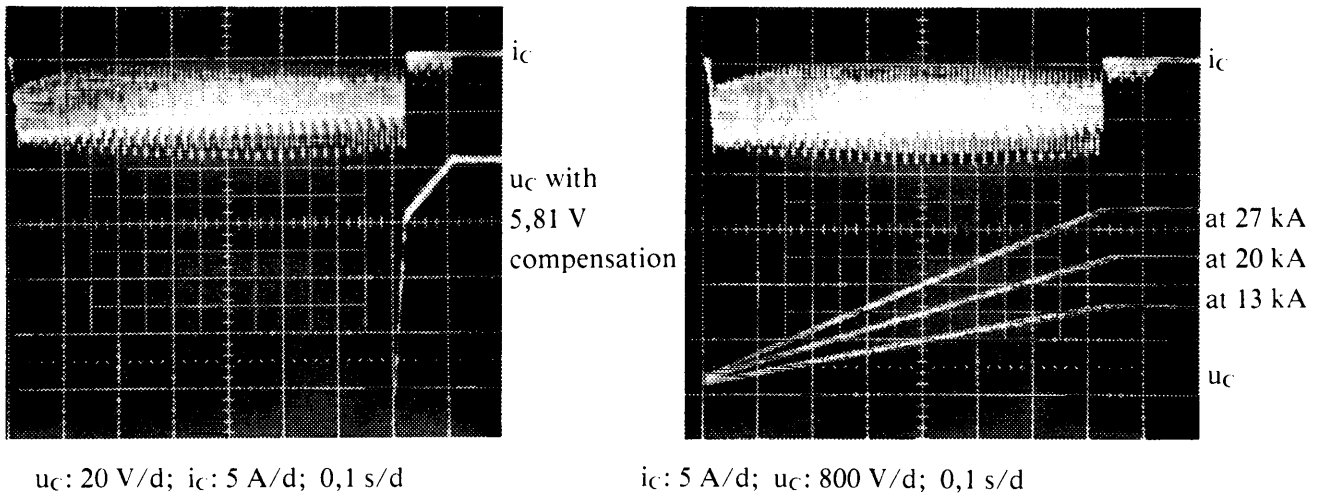
Fig. 22   Waveforms showing the double-slope capacitor voltage and double-level charging current for overshoot free voltage stabilization and constant charging time.

9.2 Corrections for magnet current amplitude modulation and irregular pulsing

Perfect linearity is assumed between charging voltage and natural discharge peak current at constant temperature.

Each discharge pulse deposits a certain amount of energy in the different parts of the load circuit — the chokes and transmission line, the pulse-matching transformer and the high-current sandwich line, the water-cooled septum winding — whose mean temperature varies in time according to their respective thermal capacitance and time constant.

The peak value of the discharge current — for a given capacitor voltage U_C — is a function of the temperature-dependent mean circuit resistance R and will consequently rapidly drift out of the working range of the active filter unless appropriate corrections are applied to $U_{C_{ref}}$.

The correction circuits are shown in Fig. 21 and the problem is treated in more detail in Appendix B.

Assuming the active filter to be out of action, four corrections are applied to obtain the proper charging voltage reference independently of the amplitude-time pattern of the current pulses within a supercycle:

20

i) The difference Δi between natural discharge current peak and flat-top reference level — and also the flat-top duration — is proportional to the charging voltage U_C. Consequently, an offset voltage $U_{C o}$ is added to limit the variation of Δi, over the working range, to a factor of ≤ 3, according to the expression:

$$\frac{\Delta i_{max}}{\Delta i_{min}} = \frac{U_{C max} + k_4 U_{C o}}{U_{C min} + k_4 U_{C o}} .$$

ii) Assuming no pulse-to-pulse amplitude modulation and a regular pulse repetition period, the variation of peak current ΔI with respect to a reference value I is proportional to the variation of resistance ΔR, which depends on the other hand on the temperature variation $\Delta\vartheta$ with respect to an initial temperature θ_0 (see Appendix B). Consequently, one can say that $\Delta I/I \sim \Delta R \sim \Delta\vartheta$ and $\Delta\vartheta \sim R\ I^2$. To obtain the temperature variation $\Delta\vartheta$ and then the $\Delta I/I$ value, a signal is elaborated by squaring and integrating the last current reference value I_n. The integration is interrupted to simulate the exponential temperature decay between successive pulses.

iii) This $\Delta I/I$ signal is multiplied by the current reference for the next pulse I_{n+1} and is converted into a final charging voltage reference according to the following expression:

$$U_{C ref} = k_6 I_{ref} + \Delta I + k_4 U_{C o} .$$

iv) Two dominating thermal time constants have been observed in the SS16 septum magnet system, one of the order of 13 s and the other of about 90 min. The first one is attributed to the higher resistance, lower thermal capacitance, water-cooled septum magnet; the second one to the more massive, natural air-convection-cooled pulse transformer and sandwich line.

If one corrects only for the shorter time constant the current peak tends to decrease very slowly. Therefore a closed loop has been introduced which maintains the active filter current inside a given window by small long-term corrections to the charging voltage reference.

Some typical signal waveforms illustrating the correction circuits described in the case of varying current reference are shown in Fig. 23.
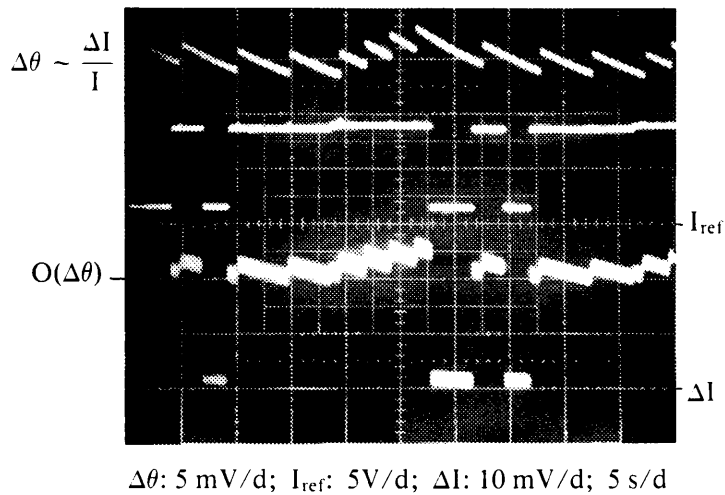

$\Delta\theta$: 5 mV/d; I_{ref}: 5V/d; ΔI: 10 mV/d; 5 s/d

Fig. 23 Typical signal waveforms of the correction circuits during a supercycle (see Fig. 21).

10. ELECTRONICS AND TIMING

The power converter can be operated under REMOTE control by computer or LOCAL control mode via the command module of its electronic crate.

The interface function between power converter and central NORD-CAMAC computer network is implemented by a digital Single Transceiver (STD) module. The CERN PS standard command and acquisition protocol is used; the states of the converter are OFF, STAND-BY, ON, RESET.

The magnet current reference is given by a 15-bit DAC and the pulsed flat top is sampled for current acquisition via a 15-bit ADC. The current analog signal is displayed in the Main Control Room via the Signal Observation System (SOS).

The electronic plug-in modules are located in a 5 U CIM crate. The main modules are the auxiliary power supply and mains synchronizing units, the thyristor gate control set, the interlocks and the command unit, the regulation and the timing modules.

The active filter control electronics and the double-pulse mode selecting circuits are located close to their respective power assemblies.

The timing function is an essential part of this type of pulsed power converter. A standard timing pulse sequence is used as defined in Table 11. Once the power converter has received an external FW pulse the sequence FW-W-ST-ME is completed either by the subsequent normal pulses or by internal guard pulses if the former were missing. This well-defined operating sequence makes sure that the capacitors are kept charged for as short a time as possible for reasons of reliability and operating life. The possibility of operating the power converter on a LOCAL timing pulses sequence is given.

Table 11

Definition of standard timing pulse sequence

Standard pulse	Function	Time delay referred to the beam (ms)	Origin
FW (Forewarning)	Initiates the capacitor charge	– 900	External CAMAC preset counter
W (Warning)	Stops the capacitor charge and inhibits the gate control set	– 10	External
ST (Start)	Triggers the HV thyristor to discharge the capacitor	– T/4[a]	Internal derived from W
ME (Measure)	Triggers the Sample-Hold (SH) and ADC circuits for flat-top current acquisition	0	External

a) T is the period of the current pulse

22

11. POWER CONVERTER CONSTRUCTION

The power section has been manufactured by an industrial firm (ALGE/A) according to a CERN technical specification [4]. The electronics has been developed and built at CERN, this being considered the most effective solution for such a small number of units (3) requiring a large amount of qualified effort, with more emphasis on performance and time schedule than on industrial grade.

The power supply consists of four modular cubicles, as shown in Fig. 5:

- a left-hand 19 in. cubicle, which containing the a.c. input switchgear and filter, the thyristor controller, the electronics crate, and the active filter power amplifier and auxiliary supply;
- the cubicle containing the HV 3-phase transformer and rectifier, the choke of the charge circuit, the third harmonic choke, the active filter choke, and the double-pulse mode power circuit;
- a double cubicle containing the energy storage capacitors and discharge components;
- finally, a right-hand 19 in. cubicle for the double-pulse mode auxiliary power supply and some other components.

12. RESULTS OF PERFORMANCE TESTS

Before final commissioning the power converters have been tested under severe operating conditions with the most stringent current amplitude modulation and irregular pulse sequence implemented by means of a μP driven programming unit.

Figure 24 shows the typical wave forms during operation at maximum current and illustrates the low-voltage stress on the magnet obtained with this type of converter.

i_m: 6 kA/d; 0,5 ms/d a)

i_m: 8 kA/d; 0,5 ms/d b)

u_m: 50 V/d; 0,5 ms/d c)
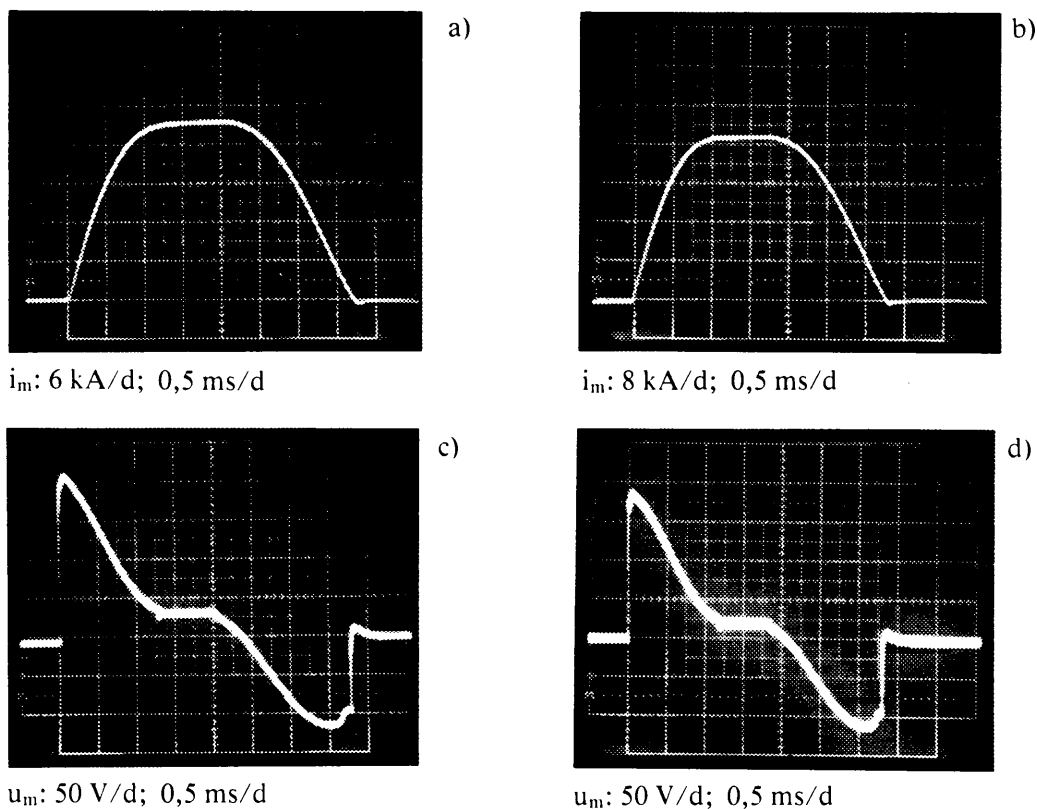
u_m: 50 V/d; 0,5 ms/d d)

Fig. 24 Typical waveforms at the maximum operational values:
a,b) current in the septum magnet (SS16 and SS58, respectively);
c,d) voltage at the feedthrough of the tank (SS16 and SS58, respectively).

23

The relevant test results for the SS16 and SS58 septum magnet systems are collected in Fig. 25.

SS16

a)

i_{AF}

i_m

i_{AF}: 100 A/d; i_m: 6 kA/d; 0,5 ms/d

b)

i_m

27 kA

(9 V)

15 A/d; 200 μs/d

c)

i_m

20 kA

(6,66 V)

15 A/d; 200 μs/d

d)

i_m

14 kA

(4.66 V)

15 A/d; 200 μs/d

e)

i_m

3,5 kA

(1,16 V)

15 A/d; 200 μs/d

SS58

f)

i_{AF}

i_m

i_{AF}: 100 A/d; i_m: 8 kA/d; 0,5 ms/d

g)

i_m

34 kA

(8,5 V)

40 A/d; 100 μs/d

h)

i_m

4,5 kA

(1,12 V)

8 A/d; 100 μs/d

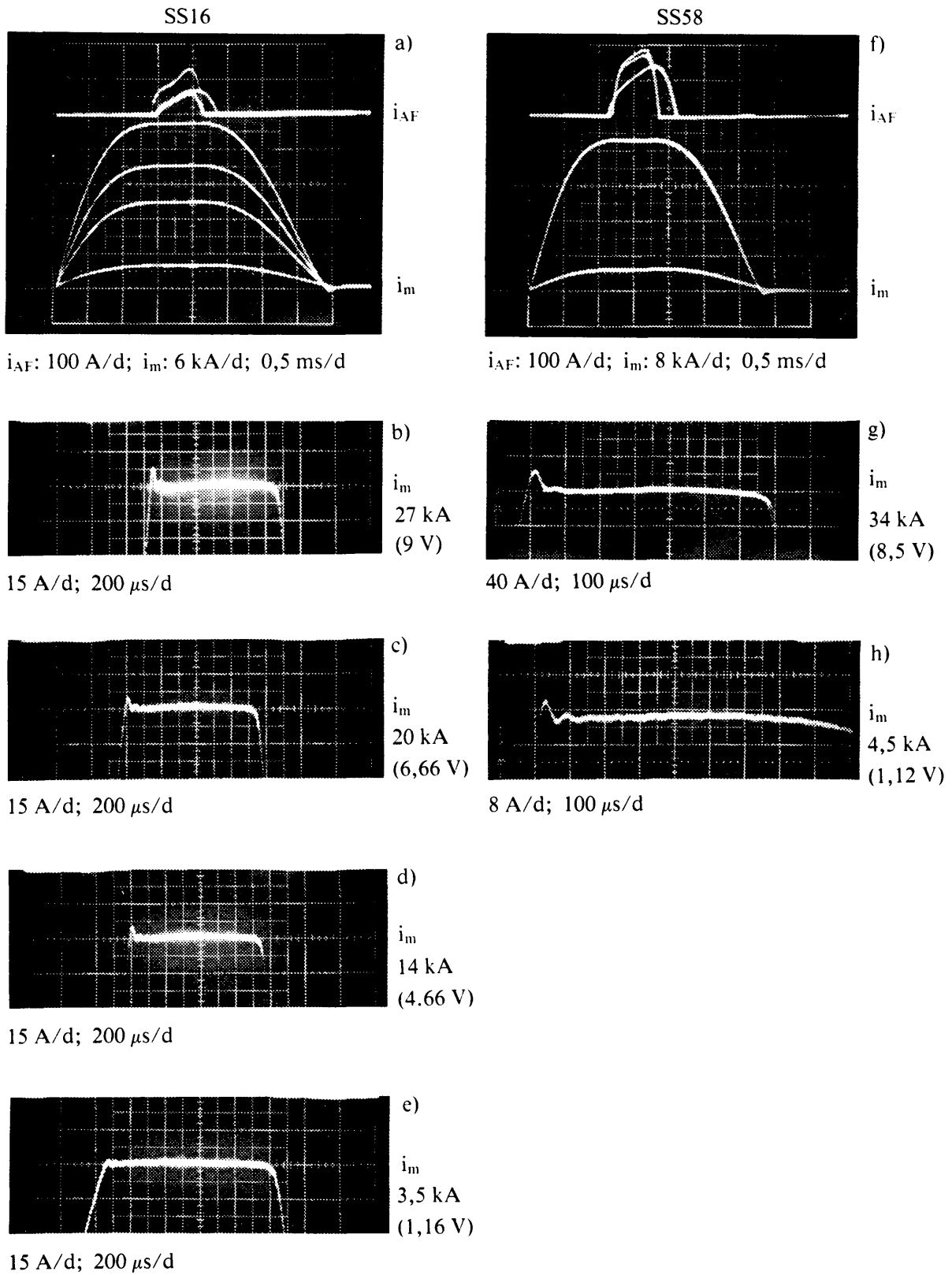Fig. 25   Test results illustrating the performance of the pulsed power converters:
a) currents in the septum magnet (SS16) and in the active filter inside the supercycle;
b), c), d), e) flat top current in the septum magnet (SS16) at 27, 20, 14 and 3.5 kA;
f) currents in the septum magnet (SS58) and in the active filter inside the supercycle;
g), h) flat top current in the septum magnet (SS58) at 34 and 4.5 kA.

13. CONCLUSIONS

The operational context of the PS accelerator complex has substantially evolved during the past five years to accelerate different kinds of particles at dedicated energies within so-called supercycles.

Unprecedented performance specifications have been satisfied by the pulsed power converter of the PS injection/ejection septum magnets in SS16 and SS58, which imply:
- current reproducibility and precision of a few parts in ten thousand, by means of a pulse flat-top current regulation,
- pulse-to-pulse current reference modulation in a 1 to 8 ratio within supercycles,
- irregular pulse repetition periods,
- double pulsing with a current flat top of 300 μs at 3.5 kA (SS16) and 4.4 kA (SS58) at 30 ms intervals.

Particular technical solutions have been developed to meet these requirements, which represent considerable progress and widen the field of application of high-stability pulsed power converters.

Some technical design aspects have been described in the report, such as the parallel type of third harmonic discharge circuit, the high-current pulse-matching transformer, the active flat-top filter, the corrections applied to cope with temperature effects on the load impedance, and the double-pulse generator.

The new power converters of the septum magnets in SS16 and SS58 have been successfully put into operation, including the double-pulse mode required for lepton operation with LEP.

---

[*] At CERN on a temporary labour contract during part of the project.

REFERENCES

[1] R. Billinge, The CERN PS complex: a multipurpose particle source, CERN/PS/83-26 (1983).

[2] J. Boillot et al., Modulation cycle à cycle des caractéristiques du faisceau et son utilisation pour le complexe d'accélérateurs du PS, CERN/PS/CO 81-16 (1981).

[3] M. Bouthéon, Opération du complexe PS en 1987, PS/OP/Note 88-10 (1988).

[4] Technical specification for capacitor discharge pulsed power converter, PS/PO SPEC 82-11 (1982).

[5] G.N. Glasoe and J.V. Lebacqz, Pulse generators, McGraw-Hill.

APPENDIX A

Design of capacitor discharge pulse-forming networks (PFN)

A current pulse with flat top and parabolic rise, as shown in Fig. A1, is obtained by superposing on the fundamental waveform an appropriate fraction of its third harmonic [5].
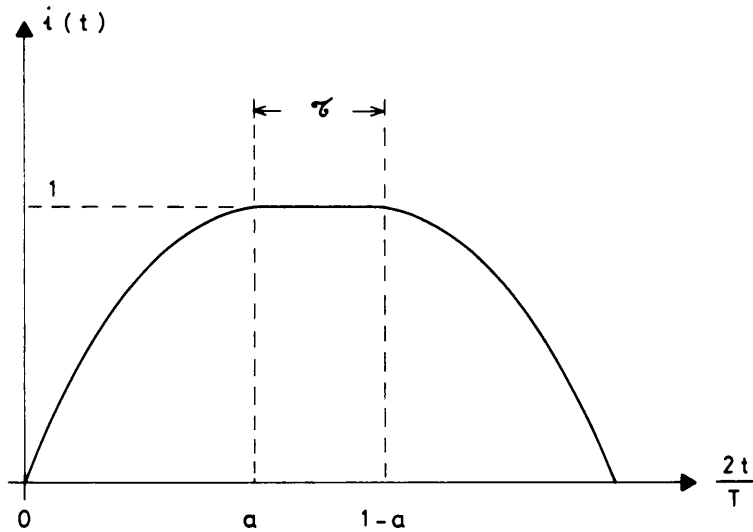
Fig. A1   Capacitor discharge current waveform.

Assuming the ideal lossless case, the expression of the current is

$$i(t) = b_1 \sin \frac{2\pi t}{T} + b_3 \sin \frac{6\pi t}{T},$$

where b_1 and b_3 are coefficients which depend on the parameter $a \simeq 0.38$ to 0.4

$$b_1 = \frac{4}{\pi} \left[\frac{\sin(\pi a/2)}{\pi a/2} \right]^2, \qquad b_3 = \frac{4}{3\pi} \left[\frac{\sin(3\pi a/2)}{3\pi a/2} \right]^2.$$

The electrical circuit which produces this discharge current waveform is shown in Fig. A2.

Fig. A2   Pulse-forming network (PFN).

The circuit components are designed according to the following relations:
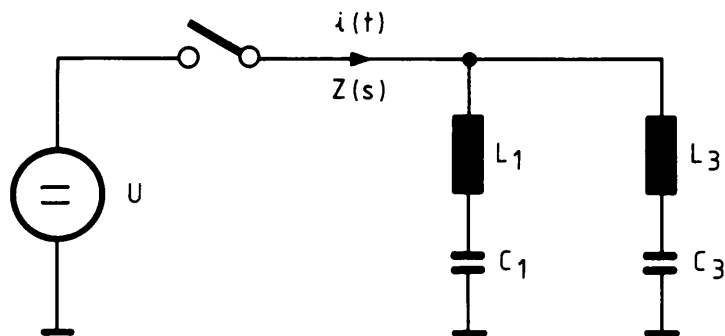
$$L_1 = \frac{Z_N\ T}{2\pi\ b_1} \ , \qquad L_3 = \frac{Z_N\ T}{6\pi\ b_3} \ ,$$

$$C_1 = \frac{T\ b_1}{2\pi\ Z_N} \ , \qquad C_3 = \frac{T\ b_3}{6\pi\ Z_N} \ ,$$

where

$$Z_N = b_1 \sqrt{\frac{L_1}{C_1}} = b_3 \sqrt{\frac{L_3}{C_3}}$$

is the normalized network impedance.

The node impedance Z(s) can be written as

$$Z(s) = \frac{A_0}{s} + \frac{A_2 s}{1 + B_2 s^2} + A_4 s \ ,$$

where

$$A_0 = \frac{C_1 + C_3}{C_1 C_3} = \frac{1}{C}$$

$$A_2 = \frac{(L_1 C_1 + L_3 C_3)(L_1 C_3 + L_3 C_1 + L_3 C_3) + L_1^2 C_1^2 + (L_1 + L_3)^2 C^2}{(L_1 + L_3)C^2}$$

$$A_4 = \frac{L_1 L_3}{(L_1 + L_3)} \frac{(C_1 + C_3)^2}{C_1 C_3}$$
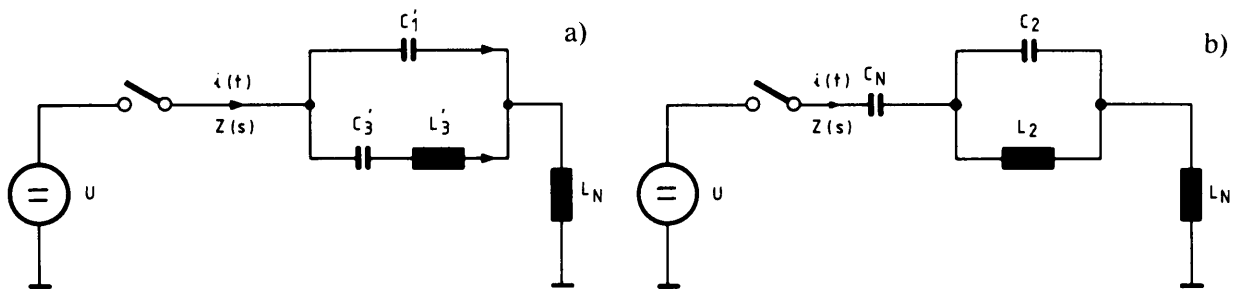
$$B_2 = (L_1 + L_3)C$$

Fig. A3   Basic a) and modified b) pulse-forming networks for septum magnet power converters.

The circuit shown in Fig. A3(a) has the same node impedance and will therefore produce the same pulse current waveform, provided that one makes

$$L_2 = A_2, \qquad C_2 = \frac{B_2}{A_2}, \qquad C_N = C_1 + C_3, \qquad L_N = \frac{L_1 L_3}{L_1 + L_3}.$$

In the case of a capacitor discharge power converter, C_N is the energy-storage capacitance and L_N the magnet load inductance.

Assuming C_N and L_N are known, the other circuit components are given by following relations:

$$\frac{C_2}{C_N} = \frac{3}{64} \frac{(b_1 + 3b_3)^2}{b_1 b_3}, \qquad \frac{L_2}{L_N} = \frac{64}{3} \frac{b_1 b_3}{(3b_1 + b_3)^2}.$$

Depending on the type of load, a modified pulse-forming network, shown in Fig. A3(b), may result in more economic components.

The equivalence between the two circuits of Fig. A3 is granted if one has:

$$C_1' + C_3' = C_N,$$

$$\frac{C_1'}{C_2} = \frac{C_3'}{C_N} = \frac{1}{n} \qquad \text{where} \qquad n = 1 + \frac{C_2}{C_N}$$

$$\frac{C_1'}{C_3'} = \frac{C_2}{C_N} = n - 1, \qquad \frac{C_3'}{C_2} = \frac{1}{n(n-1)}, \qquad \frac{L_3'}{L_2} = n^2.$$

To facilitate the circuit design, in both cases, the parameters C_2/C_N and L_2/L_N as well as C_1'/C_N, C_3'/C_N, and L_3'/L_M have been plotted against the parameter a in Fig. A4.
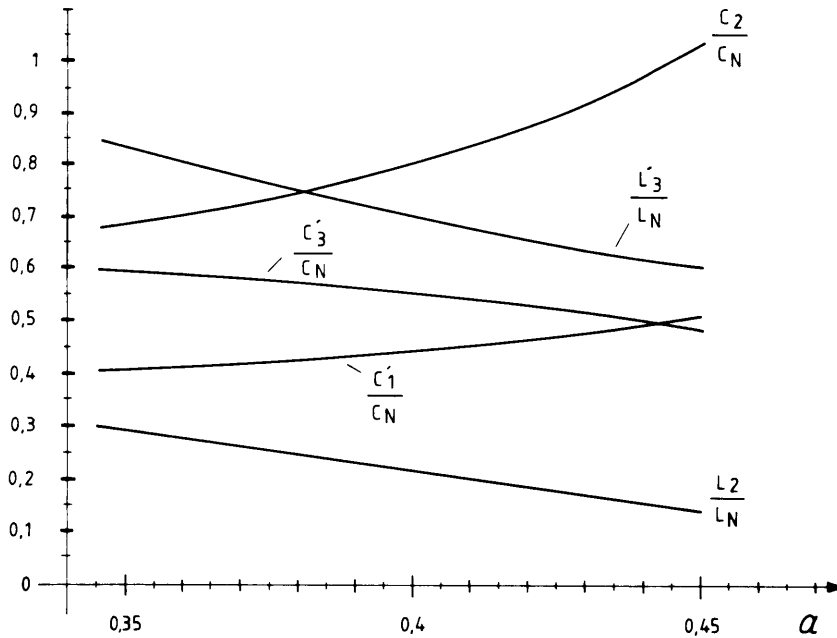

Fig. A4 Parameters C_2/C_N and L_2/L_N of the basic PFN and C_1'/C_N, C_3'/C_N, L_3'/L_N of the modified PFN as function of a.

Table A1 shows the theoretical discharge circuit components of the power converter according to Fig. A4 ($a = 0.4$).

Table A1

Theoretical values of discharge circuit components

	$L_N^{*)}$ (μH)	C_N (μF)	L_2 (μH)	C_2 (μF)	L_3' (μH)	C_3' (μF)	C_1' (μF)
SS16	720	1200	166	930	524	676	524
SS58	504	1200	116	930	367	676	524

*) This refers to the primary of the pulse-matching 12:1 transformer.

The relevant current and voltage waveforms of the two types of pulse-forming networks are shown for comparison in Fig. A5.
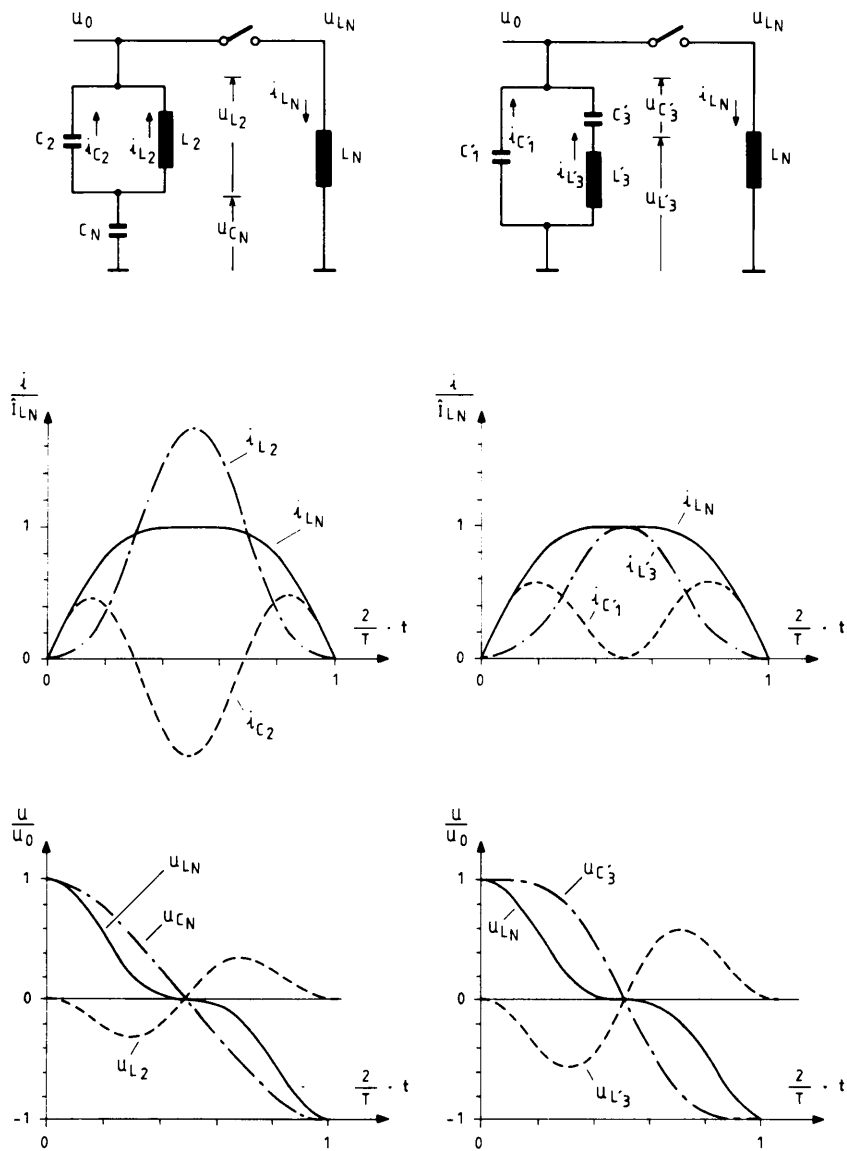

Fig. A5   Current and voltage waveforms of basic and modified PFN.

APPENDIX B

Correction of temperature-dependent load impedance variations

The problem consists in having, at any time within the supercycle sequence the correct capacitor voltage reference which will at the next pulse produce the desired septum magnet current.

The load is considered to consist of two parts:

i) the forced water-cooled monoturn septum winding, and

ii) the natural air-convection-cooled transformer and sandwich line.

The following expressions apply:

$$I \approx \frac{U_c}{\omega L} \exp\left(-RT/8L\right) \qquad \text{for the peak pulse current and} \qquad \frac{\Delta I}{I} \sim -\frac{T}{8L} \Delta R \sim -\frac{T}{8L} \cdot \alpha \cdot \Delta\vartheta$$

for the relative current variation due to a variation of load resistance ΔR and of temperature $\Delta\vartheta$—with respect to initial values R_0 and ϑ_0—when the pulse occurs; α being the temperature coefficient of the material.

The evolution of load temperature within a supercycle is schematically shown in Fig. B1 for regular pulsing and in the more general case of amplitude and frequency modulation.
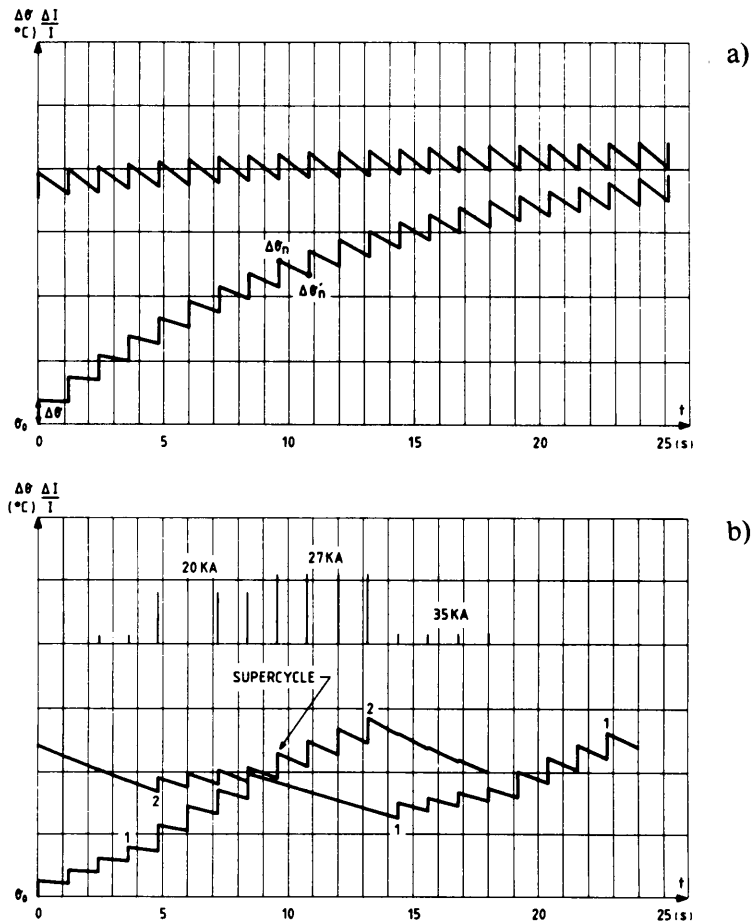

Fig. B1 Schematic representation of the load temperature evolution during a supercycle.
   a) regular pulse repetition frequency with constant reference.
   b) general case.

To compute the temperature increase $\Delta\vartheta_n$ just after the nth pulse or $\Delta\vartheta_n'$ just before the $(n+1)^{th}$ pulse one can express the temperature in terms of transient thermal impedance Z_{th} for the pulse duration and apply the superposition principle to a train of pulses of power P_m at a time interval T_r

$$\Delta\vartheta_n = Z_{th} \sum_{m=1}^{n} P_m \exp[-(n-m) T_r/\tau]$$

$$\Delta\vartheta_n' = Z_{th} \sum_{m=1}^{n} P_m \exp[-n-m+1) T_r/\tau] \quad.$$

The power P_m is given by $[R_m (I_m^2/2)]$ with $R_m = R_0(1 + \alpha\Delta\vartheta_{m-1}')$.

For identical current pulses of power P one can write:

$$\Delta\vartheta_n = Z_{th} P \sum_{m=1}^{n} \exp[-(n-m) T_r/\tau]$$

$$\Delta\vartheta_n' = Z_{th} P \sum_{m=1}^{n} \exp[-(n-m+1) T_r/\tau]$$

and for the expected relative variation of the $(n+1)^{th}$ current pulse:

$$\frac{\Delta I_{n+1}}{I_{n+1}} \sim I_n^2 \frac{e^{-T_r/\tau}}{(1-e^{-T_r/\tau})} \quad.$$

Finally the correction for the $(n+1)^{th}$ pulse is given by

$$\Delta I_{n+1} \approx I_n^2 I_{n+1} \frac{1}{(e^{T_r/\tau}-1)} \quad.$$

The time constant τ for the exponential temperature decrease during the time T_r between pulses can be derived if one measures the current pulse variation for a given current and two different pulse repetition periods (T_r and $2T_r$, for example 1.2 and 2.4 s):

$$\frac{(\Delta I)_{T_r}}{(\Delta I)_{2T_r}} = e^{T_r/\tau} + 1 \quad \text{and finally} \quad \tau = \frac{T_r}{\ln[(\Delta I)_{T_r}/(\Delta I)_{2T_r} - 1]} \quad.$$
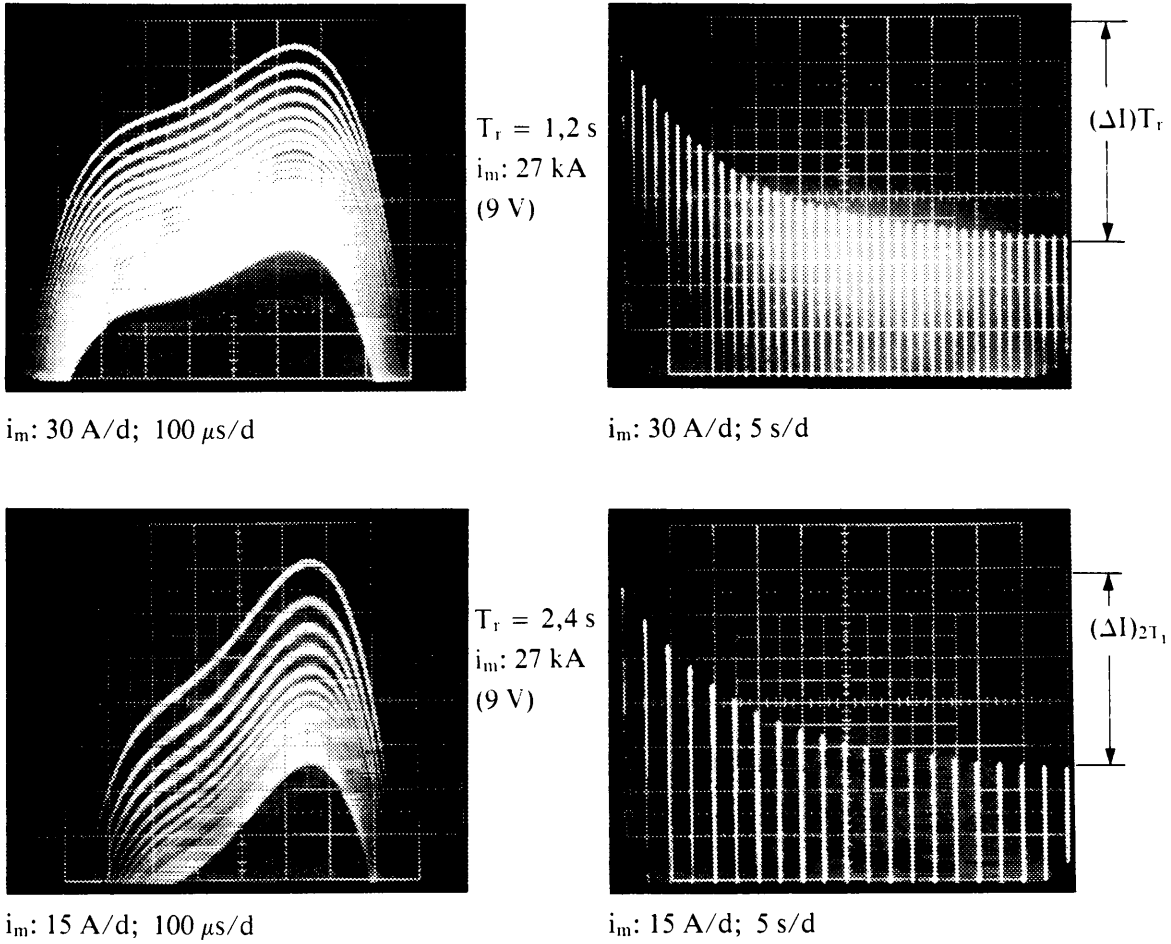
This procedure is shown in Fig. B1 for the SS16 system.

T$_r$ = 1,2 s
i$_m$: 27 kA
(9 V)

i$_m$: 30 A/d; 100 μs/d

i$_m$: 30 A/d; 5 s/d

$(\Delta I)T_r$

T$_r$ = 2,4 s
i$_m$: 27 kA
(9 V)

i$_m$: 15 A/d; 100 μs/d

i$_m$: 15 A/d; 5 s/d

$(\Delta I)_{2T_r}$

Fig. B2   Determining the thermal time constant τ of the SS16 system by pulsing at 27 kA with regular pulse repetition periods of 1.2 and 2.4 s.

The above method applied to the SS16 system gives a time constant τ of ~ 13 s. Another method of determining τ consists in heating up the system to 27 kA with a 1.2 s pulse repetition period, in reducing the current to 3.5 kA, where the energy deposited by each pulse is negligible, and in observing the evolution of the current peak. The two methods give the same τ to within 10%.

33